

Article

Understanding Geodiversity for Sustainable Development in the Chinchiná River Basin, Caldas, Colombia

Alejandro Arias-Díaz ^{1,2,3} , Hugo Murcia ^{1,2,4} , Felipe Vallejo-Hincapié ^{1,2,3}  and Károly Németh ^{5,6,*} 

¹ Instituto de Investigaciones en Estratigrafía (IIES), Universidad de Caldas, Manizales 170001, Colombia; alejandro.arias5660@ucaldas.edu.co (A.A.-D.); hugo.murcia@ucaldas.edu.co (H.M.); diego.vallejo@ucaldas.edu.co (F.V.-H.)

² Grupo de Investigación en Estratigrafía y Vulcanología (GIEV) Cumanday, Universidad de Caldas, Manizales 170001, Colombia

³ AURORA, Science Communication SAS, Manizales 170001, Colombia

⁴ Departamento de Ciencias Geológicas, Universidad de Caldas, Manizales 170001, Colombia

⁵ Saudi Geological Survey, Jeddah 21514, Saudi Arabia

⁶ Institute of Earth Physics and Space Science, H-9400 Sopron, Hungary

* Correspondence: knemeth69@gmail.com or k.nemeth@massey.ac.nz

Abstract: Geodiversity, comprising both endogenous and exogenous geological processes, plays a crucial role in shaping the structure and functionality of natural systems, alongside its substantial impact on human well-being. However, the often-overlooked interconnection between geodiversity components limits our comprehension of geosystems. In the Chinchiná River Basin (CRB) in Colombia, located in the northern Andes in South America, we established criteria to differentiate geodiversity classes, calculated indices to understand the distribution of geological elements, and discussed systemic relationships. This comprehensive approach lays the foundation for a holistic comprehension of the territory's structure and functionality. Our findings revealed the convergence in an area of 1052 km² of 10 rock types, 7 slope ranges, 13 landforms, 5 drainage density features, 610.4 km of faults with 9 kinematic tendencies, 5 soil orders, 5 climate types, a 3328 km surface drainage network with 7 hydrographic orders, 1 underground aquifer, 4 areas with lakes, 2 zones with glaciers, 27 polygenetic and monogenetic volcanoes, and several thermal springs. This discussion explores the implications of various methodologies used to establish the value of the general geodiversity index while also examining the relationships between abiotic elements and their distribution patterns. This forms a fundamental basis for understanding the geosystem services of the basin in terms of regulation, support, and provisioning processes, as well as the culture and knowledge derived from geodiversity. These conceptual elements are indispensable for enhancing the sustainability of a region that is susceptible to the impacts of climate change. Furthermore, they serve as the foundations for the objective's achievement, as set by the UNESCO Global Geopark project "Volcán del Ruiz", currently ongoing within the region.

Keywords: geodiversity quantification; geodiversity index; geosystem services; sustainability; northern Andes



Citation: Arias-Díaz, A.; Murcia, H.; Vallejo-Hincapié, F.; Németh, K. Understanding Geodiversity for Sustainable Development in the Chinchiná River Basin, Caldas, Colombia. *Land* **2023**, *12*, 2053. <https://doi.org/10.3390/land12112053>

Academic Editors: Murray Gray, Paulo Pereira and Maria da Glória Garcia

Received: 2 October 2023

Revised: 9 November 2023

Accepted: 10 November 2023

Published: 11 November 2023



Copyright: © 2023 by the authors. Licensee MDPI, Basel, Switzerland. This article is an open access article distributed under the terms and conditions of the Creative Commons Attribution (CC BY) license (<https://creativecommons.org/licenses/by/4.0/>).

1. Introduction

Earth is a complex functional system where biotic and abiotic elements play roles in the diversity of nature [1–3]. Although nature structures and functionalities depend on the interconnections and interdependencies of both biodiversity and geodiversity, the former has been widely prioritized over the latter in terms of nature conservancy [4,5]. This has led to the exclusion and underestimation of abiotic elements, resulting in a limited perspective on the holistic value of nature [6,7]. Geodiversity refers to the natural diversity of the Earth's surface with regard to geology (rocks, minerals, volcanoes, fossils, etc.), geomorphology (landforms, topography, physical and anthropogenic processes), hydrology,

soil, and climatology, including their associations, structures, processes (endogenous and exogenous), systems, and contributions to the landscape [1,8,9]. The capacity of a region to host natural variety is linked to the circumstances and characteristics of geodiversity [1,5,9]. Thus, geodiversity is an intrinsic property of the territory, ensuring the sustenance of life on Earth and maintaining the functionalities of ecosystems and their services [10,11]. The geodiversity also helps to regulate geochemical cycles and provides materials, energy, water, food, and various resources, including cultural and knowledge-based assets, all of which enhance the well-being of human societies [12,13]. All these benefits derived from geodiversity are known as geosystem services, which are differentiated from ecosystem services based on three fundamental aspects: space, scale, and time (i.e., geosystem has been shaped over geological time by processes that tend to be of greater magnitudes than ecosystem dynamics) [7,12].

Despite its undeniable importance, geodiversity confronts various methodological challenges, largely due to its multifaceted nature, the multiple ways in which it can be studied, and the various conditioning factors of the results [14]. When comparing various authors, distinctions become evident in terms of the number and types of geodiversity classes and subclasses that they use (i.e., sets of geological elements within a region and the standard criteria used to distinguish between objects), the varying methodologies employed for index calculations, and the disparate scales and sizes of the study areas that they investigate [15–26]. Therefore, it becomes crucial to establish a well-defined methodological and informational framework to guide geodiversity assessment. However, increasing geodiversity research, coupled with the urgent need to integrate with biodiversity, as well as give insights into the geosystem services, constitutes an opportunity to strengthen the sustainability of territories by providing the abiotic component required for a more complete conception of nature. This holds particular significance for tropical regions in the northern Andes, given their exceptional biodiversity and sensitive vulnerability to the impacts of global climate change [27,28]. In particular, this framework is useful in places where a comprehensive assessment of geodiversity has never been conducted but is necessary due to various ongoing dynamics (e.g., linked to the UNESCO Global Geopark project “Volcán del Ruiz”, which focuses on preserving geological and natural heritage).

The Chinchiná River Basin (CRB) is a tropical fluvial basin in the northwestern Andes in Colombia, South America (Figure 1). The CRB belongs to the Magdalena and Cauca basins, which are among the most important rivers in the country because of their contribution to the country’s gross domestic product [29,30] (Figure 1A). One of the most important eastern tributaries of the Cauca River is the Chinchiná River, located at western flank of the Central Cordillera of Colombia in the south-central region of the Department of Caldas (Figure 1A–C). The CRB has an extension of 1051 km² and is composed of three sub-basins (i.e., the Guacaica River Sub-Basin, Chinchiná River Sub-Basin, and Claro River Sub-Basin) (Figure 1C), which together comprise five political administrative areas that host ~525,800 inhabitants: the Manizales, Villamaría, Chinchiná, Palestina, and Neira municipalities (Figure 1B).

In this study, several parameters were determined to define and characterize the geodiversity classes and sub-classes of the CRB. The geological criteria used for distinguishing abiotic elements are explained in the methodology, with the results section providing a detailed description of these criteria. Statistical methods were used to find a general geodiversity index through the sum of different geodiversity sub-indices, each referring to the number of abiotic elements per unit of territory for each of the CRB geodiversity classes. Additionally, this process was complemented by an evaluation of the significance of the diversity observed within each geographic unit of analysis in relation to the total potential abiotic diversity identified within the basin. This index was used to determine the type, number, and distribution of geodiversity elements and define, under a previously established framework, where the highest amount of geodiversity was concentrated in the study area. Then, the distribution patterns of the indices were analyzed and discussed, along with the factors and circumstances that condition them. Hence, through the examina-

tion of the inter-relationships between geodiversity classes, certain foundational aspects of geosystem services were qualitatively outlined. This process provided a framework for enhancing our comprehension of the territory.

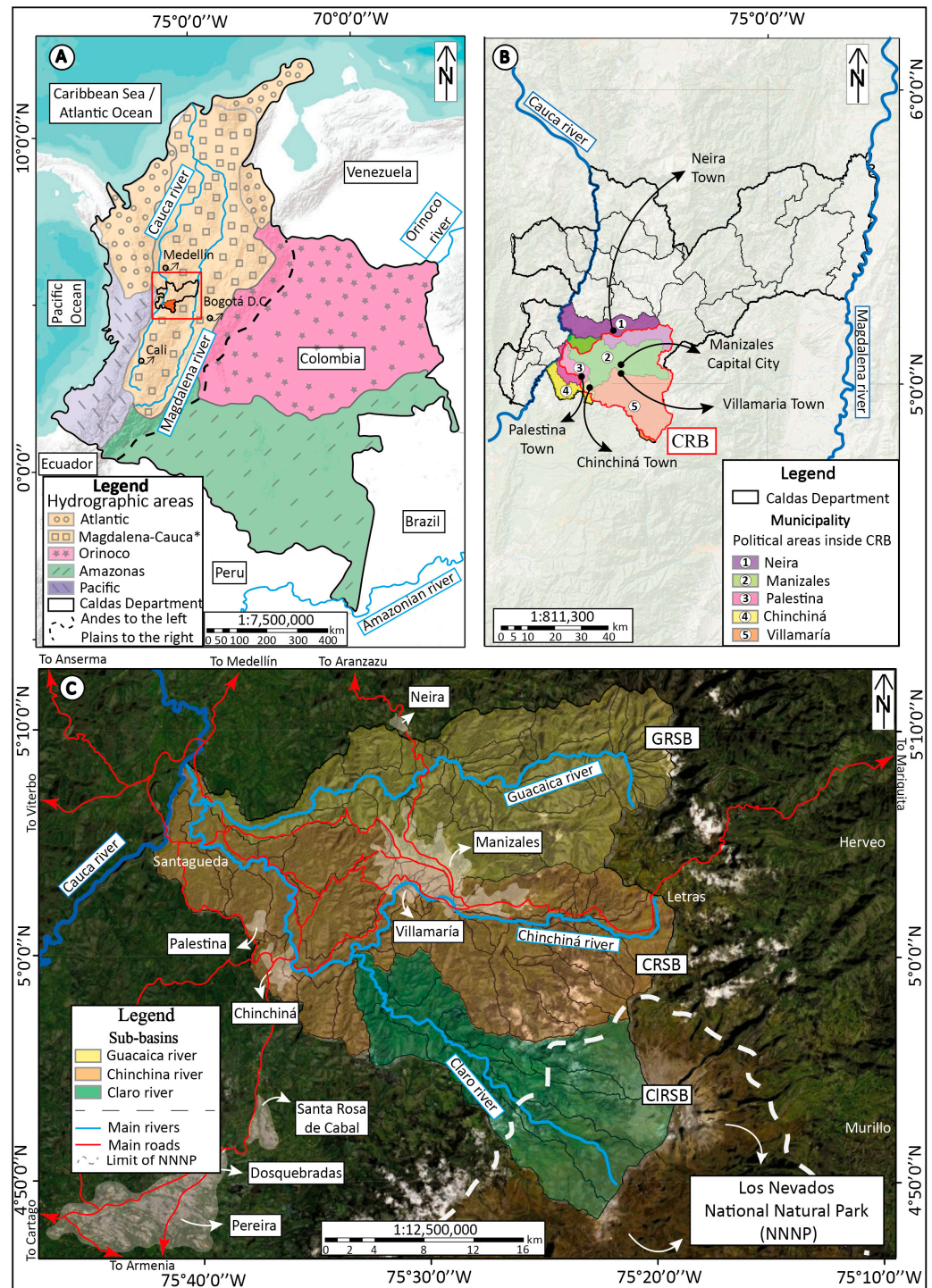


Figure 1. (A) Hydrographic areas of Colombia (* Magdalena–Cauca belonging to the Atlantic hydrographic area). Modified from Esri, USGS, and NOAA. (B) Caldas department and its municipalities, and the localization of the Chinchiná River Basin and political administrative areas inside the basin. Modified from Esri, Garmin, GEBCO, and NOAA NGDC. (C) Sub-basins of the Chinchiná River Basin. Modified from Esri, Maxar, GeoEye, Earthstar Geographics, CNES/Airbus DS, USDA, USGS, AeroGRID, IGN, and the GIS user community.

2. Geosystemic Framework

The CRB is characterized by diverse geological features and environmental phenomena. It encompasses various rock types, including igneous, metamorphic, and sedimentary rocks, as well as volcanoclastic deposits, which are the result of the tectonic evolution of northwestern South America (Figure 2B). This evolution has included the collision of several allochthonous terranes, through multiple fault systems and at different times, into the Amazonian craton [31–34]. The present tectonic framework is controlled by combined processes associated with the Nazca Plate, South American Plate, and Caribbean Plate (Figure 2A) [35–38].

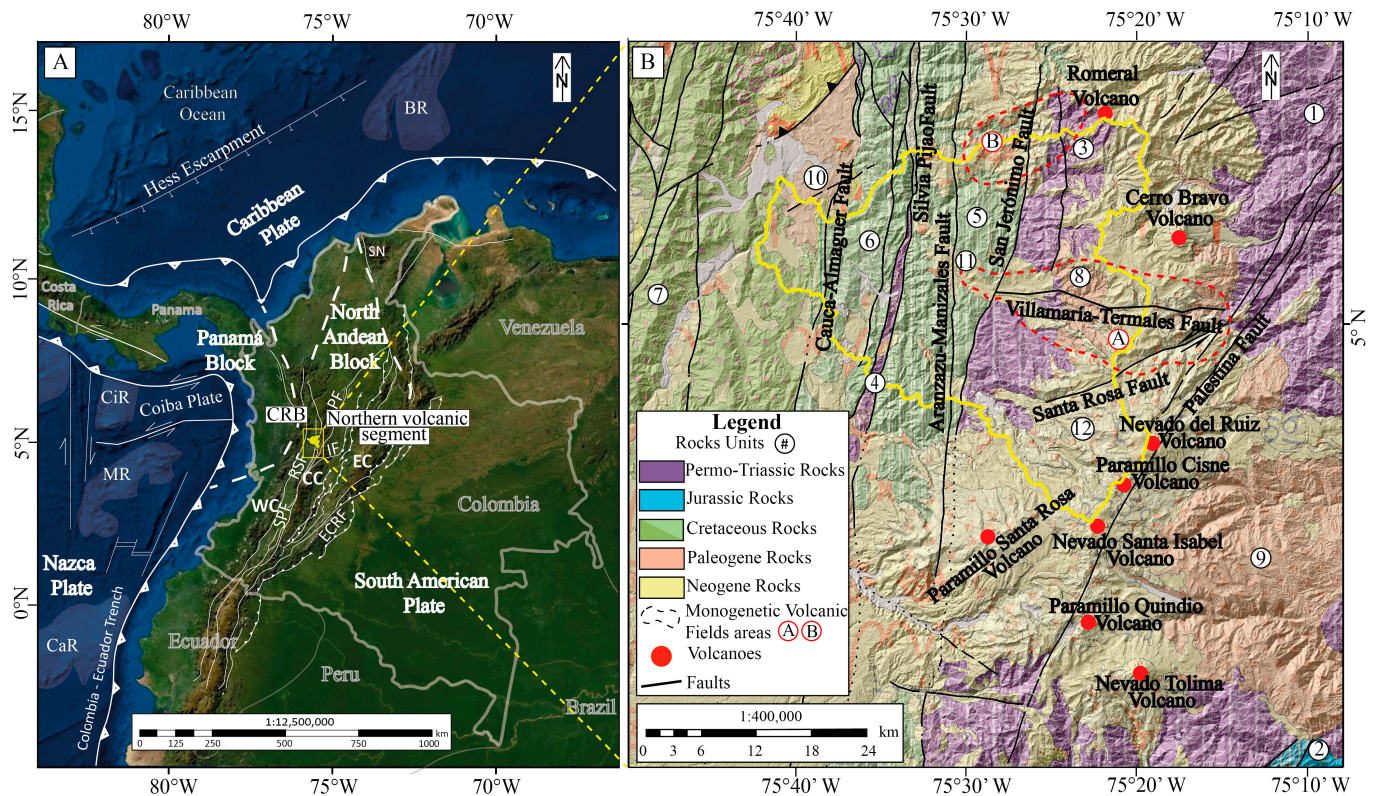


Figure 2. (A) Tectonic framework—CRB: Chinchina River Basin; CC: Central Cordillera; WC: Western Cordillera; EC: Eastern Cordillera; SPF: Silvia Pijao Fault; RSF: Romeral System Fault; IF: Ibagué Fault; PF: Palestina Fault; SN: Sierra Nevada; ECRF: Eastern Colombian Range Fault; CaR: Carnegie Ridge; MR: Malpelo Ridge; CiR: Coiba Ridge; CoR: Cocos Ridge; BR: Beata Ridge. [39,40]. Modified from Esri, Maxar, GeoEye, Earthstar Geographics, CNES/Airbus DS, USDA, USGS, AeroGRID, IGN, and the GIS user Community. (B) Geological map of the region—1: Cajamarca complex, 2: Ibagué batholith, 3: Granitic milonite of Guacaica, 4: Chinchiná-Santa Rosa stock, 5: Quebradagrande complex, 6: Arquía complex, 7: Barroso formation, 8: Manizales stock, 9: The Bostque batholith, 10: Irra-Tres Puertas formation, 11: Volcanoclastic flows, 12: Quaternary deposits, “A”: Villamaria-Termiales monogenetic volcanic field, “B”: Tapias-Guacaica monogenetic volcanic field. Adapted from [41].

The CRB is in the Northern Andean Volcanic Zone, or more specifically in the Northern Volcanic Segment of Colombia, which was formed by the Nazca oceanic lithospheric plate subduction under northern South America [40,42] (Figure 2A). This allows the formation of several polygenetic and monogenetic volcanoes, including the iconic Nevado del Ruiz Volcano [43–53] (Figures 2B and 3A–D). The basin’s tectonic history and ongoing orogenic activity in the region has created multiple fault systems that govern its steep and diverse topography. The Cordillera’s high slopes merge with volcanoes to define the varied geomorphology [54] (Figure 3A,D–F). The distribution, location, and surface manifestation of

volcanoes in the area have been significantly influenced by structural control, as some of the fault systems have served as conduits for the ascent of magma [55]. Fractures within the rocks guide water infiltration, which, in conjunction with the magmatic context thermal gradient, heats up water and forms hydrothermal fluids rich in salts and metals, which, in addition to altering the rocks and forming various minerals of economic interest, produce thermal manifestations on the surface [56–58] (Figure 3B,C). Climatologically, the CRB is strongly influenced by altitudinal factors, such as temperature, precipitation, solar brightness, relative humidity, and solar radiation change with altitude [59,60] (Figure 3D,E,G). Two of the six remaining glaciers in Colombia can be found in the CRB, nourishing the paramo ecosystem, which is recognized for its special water retention capacity, which feeds the downstream rivers, lakes, and aquifers throughout the basin [59–62] (Figure 3G).



Figure 3. (A) Southeastern panoramic view of the basin: polygenetic and monogenetic volcanoes, as well as some fault systems of the Chinchiná River Basin. (B) Hot spring thermal waters from inside the rocks. Intense alteration colors are visible around the thermal manifestation. (C) Highly hydrothermally altered rock outcrop. (D) Monogenetic volcanic domes influencing the relief and topography of the basin. (E) Hillsides, valleys, and slopes dissected by the drainage network, which produced a steep relief. (F) Large valleys oriented north–south by the structural control of regional faults. (G) Glacier border of Nevado Santa Isabel. Photo credit: Aurora Sciences Communication (SAS).

3. Materials and Methods

A multivariate methodology was employed to quantitatively assess the geodiversity of the CRB, combining the methodological principles proposed by [20–22]. Geodiversity classes were considered, including lithologies, geomorphology, pedology, structural geology, hydrology, climate, volcanoes, and geothermal hot springs. In this study, climate is considered to be a form of geodiversity, given its significant variability within the basin, derived from the substantial variation in altitude. Concurrently, it was necessary to exclude the paleontological and mineralogical classes from quantification due to the scarcity of detailed information available. Specific criteria were established to differentiate between the component abiotic elements and group them into subclasses (Table 1). A geodiversity sub-index was calculated for each of the classes, following particular specifications (Table 1). In general, these indices represented a count of abiotic elements per unit area, and calculations were performed utilizing the ArcGIS tool developed by [63] (Figure 4). The territory was segmented into analytical units with two distinct grid sizes (i.e., 1 km × 1 km and 2 km × 2 km) (Figure 4A). This dual-grid approach allowed us to examine the influence of the unit size variations on the calculated index. The general geodiversity index was obtained by summing the calculated sub-indices for each of the eight classes.

Table 1. Geodiversity classes, criteria definition, geodiversity subclasses, abiotic elements, sub-index parameters, and information source. Modified from [63].

Geodiversity Classes	Differentiation Criteria of Subclasses	Geodiversity Subclasses	Abiotic Elements	Sub-Index Parameters	Information Source
Lithological	Age, composition, and/or genesis of the rocks and deposits	Igneous Metamorphic Sedimentary Volcanosedimentary	Paleogene intrusive rocks Mesozoic volcanic rocks Cenozoic volcanic rocks Permian metamorphic rocks Triassic metamorphic rocks Cretaceous metamorphic rocks Cretaceous metasedimentary rocks Mesozoic sedimentary rocks Cenozoic sedimentary deposits Cenozoic volcanosedimentary deposits	Defined as the number of abiotic lithological elements represented on the geological map per unit area	The lithological map was acquired from Colombian Geological Survey [64–66]; additionally, the andesitic bodies of the Villamaría Termales monogenetic volcanic field and the Tapias Guacaica monogenetic volcanic field were included [46,47,51], and the scale of this map is 1:100,000.
Geomorphological	Morphometric parameters	Slopes ranges	Flat to slightly flat (0–1.7°) Slightly inclined (1.7–4°) Moderately inclined (4–7°) Strongly inclined (7–14°) Slightly steep (14–26°) Moderately steep (26–36°) Steep (>36°)	Corresponds to the number of different abiotic geomorphological elements per unit area	The slopes' ranges and drainage densities were developed utilizing ArcGIS software 10.8 using the 12.5 m DEM; the landforms were adapted from [67], and the scale of this map is 1:25,000.
		Landforms	Andean summits Dome Flood Plain Hills Hilly Terrain Lava Flow Mudflow and lahar Narrow Valley Narrow mountain range Sloping terrain Terrace Volcanic cone Anthropogenic geomorphology		
		Drainage density	Very low Low Medium High Very High		

Table 1. Cont.

Geodiversity Classes	Differentiation Criteria of Subclasses	Geodiversity Subclasses	Abiotic Elements	Sub-Index Parameters	Information Source
Structural	Fault kinematics and the strike and/or dip movement component	Dextral Sinistral Reverse Normal	Dextral Dextral normal Sinistral Sinistral inverse Reverse Reverse dextral Reverse sinistral Normal Normal sinistral	It was defined as the number of faults per unit area	The structural map was adapted from [55], and the scale of the map is 1:100,000
Pedological	Chemical, physical, and mineralogical composition	Soil order No soil formation Urban soil	Andisols Inceptisols Mollisols Histosols Entisols No soil formation Urban soil	The calculation of this index was made by counting the pedological order in the soil map per unit area	The pedological map was adapted and modified from [67], and the scale of this map is 1:25,000
Climatological	Elevation, mean annual temperature, and mean annual total precipitation	Snow Paramo Cold Temperate Warm	Permanent snow cover Superhumid high paramo Superhumid low paramo Low humid paramo Cold Superhumid Cold wet Temperate moist Temperate semihumid Warm humid Warm semihumid	Corresponds to the number of abiotic climatical elements per unit area	The climatic zones were taken from [61]
Hydrographical	Surface and groundwater conditions	Stream order Aquifers Lakes Glaciers	Seven stream orders One aquifer Four lake areas Two glaciers	The highest order of hierarchy present in each unit area was divided by two (approximating it to the nearest whole number if it is a decimal), and we added the presence of aquifers, glaciers, and lakes	The stream orders were developed via ArcGIS software 10.8 using the 12.5 m DEM, and applying the Strahler method, while the aquifer information was taken from www.corpocaldas.gov.co (accessed on 16 february 2023), and the lakes and glaciers were identified during field work; the scale of this map is 1:100,000.
Volcanological	Type of volcano	Polygenetic Monogenetic	Five polygenetic Twenty two monogenetic	This class works as the counting of volcanoes per unit area	The volcanological map was developed from information collected in several studies [46,47,50–53], and the scale of this map is 1:100,000
Geothermal	Temperature ranges	<35 °C 35–70 °C >70 °C	Three hot springs below 35 °C Eleven hot springs between 35 °C and 70 °C Two hot springs upward from 70 °C	It is defined as the counting of hot springs' temperature ranges per unit area	The geothermal diversity map was derived from [56]

We conducted an additional analysis of the results. Statistical processing revealed the geodiversity percentage for each geographic analysis unit using class equivalences. This procedure helped us to determine the relative sub-index percentages for each class in relation to the total count of abiotic elements within each class. To take this step, we initially established the equivalence of sub-indices for each class.

$$\text{Sub-index equivalence per class (SBEC)} = \text{sub-index} \times 100 / \text{Total class abiotic elements} \quad (1)$$

The sub-indices were then weighted based on the equivalent percentage for each class, with each class considered to have equal importance in the overall geodiversity (i.e., since we assessed eight classes, each class was assigned a weight of 12.5%):

$$\text{Sub-index equivalence per total geodiversity} = (\text{SBEC}) \times 12.5\% / 100 \quad (2)$$

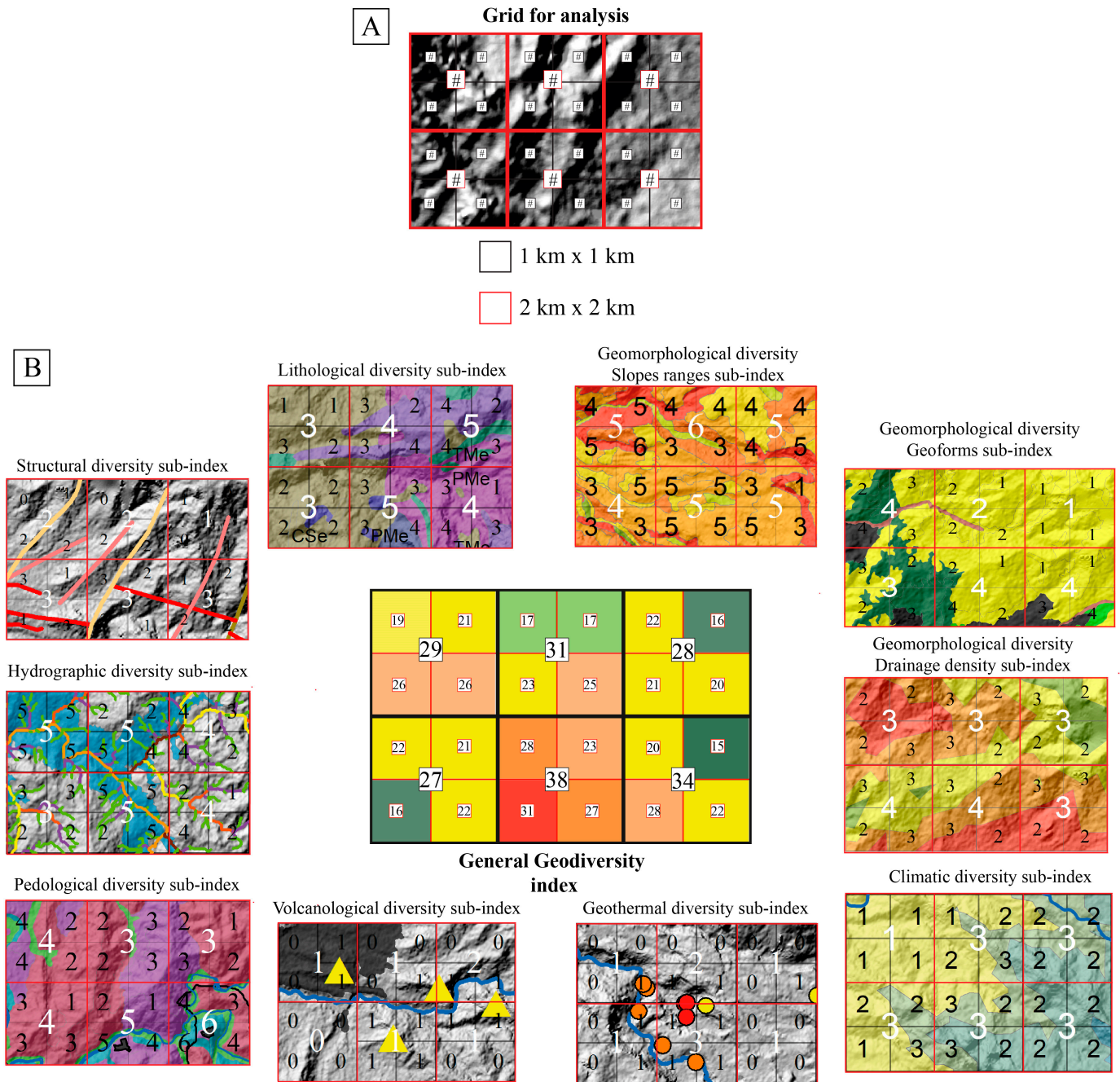


Figure 4. (A) Grid used for analysis of the territory. (B) Graphical examples of the geodiversity sub-indices and the general sum of the general geodiversity index. Black/small numbers correspond to the 1 km × 1 km index, whereas the white/big numbers correspond to the 2 km × 2 km index.

It is important to clarify that our analysis aimed to identify the presence of abiotic elements and their distribution, with no intention of attributing value or significance to specific categories. Therefore, we opted to assign equal weight to each class. Nevertheless, following the statistical process, each class assumed a distinct value within the overall geodiversity, as its respective contribution to the total was established based on the total count of abiotic elements (Table 2). This analysis provides insight into the comprehensive geodiversity present within each analyzed geographic unit, encompassing all the identified abiotic diversity present in the CRB.

Table 2. Statistical weighting of sub-indices and geodiversity classes.

Geodiversity Class	Total Abiotic Elements	Class Sub-Index	Sub-Index Equivalence per Total Abiotic Elements per Class	Sub-Index Equivalence in Total Geodiversity
Lithological	10	1	10%	1.25%
		2	20%	2.5%
		3	30%	3.75%
		4	40%	5%
		5	50%	6.25%
		6	60%	7.5%
Geomorphological	25	5	20%	2.5%
		6	24%	3%
		7	28%	3.5%
		8	32%	4%
		9	36%	4.5%
		10	40%	5%
		11	44%	5.5%
		12	48%	6%
		13	52%	6.5%
Structural	9	1	11%	1.4%
		2	22%	2.8%
		3	33%	4.2%
		4	44%	5.6%
Pedological	7	1	14.3%	1.8%
		2	28.6%	3.6%
		3	42.9%	5.4%
		4	57.1%	7.1%
		5	71.4%	8.9%
Climatological	11	1	9.09%	1.13%
		2	18.18%	2.72%
		3	27.27%	3.40%
		4	36.36%	4.54%
Hydrological	7	1	14.3%	1.7%
		2	28.6%	3.5%
		3	42.9%	5.35%
		4	57.1%	7.14%
		5	71.4%	8.9%
Volcanological	2	1	50%	6.2%
		2	100%	12.4%
Geothermal	3	1	33.33%	4.16%
		2	66.66%	8.3%
		3	100%	12.5%

Below, a detailed description of the subclasses is provided, along with the calculation of each geodiversity sub-index. This is followed by the presentation of the overall geodiversity index. Then, methodological considerations are discussed, as are distribution patterns and qualitative relationships between the geodiversity elements within the CRB.

4. Results

4.1. Geology

4.1.1. Geological Diversity of the Chinchiná River Basin

- Igneous subclass

The igneous rocks of the basin are divided into Paleocene plutonic rocks, which correspond to the tonalites and granodiorites of the Manizales Stock [65,68,69], covering

an area of 34.23 km² (i.e., 3.23%), and are located in the central-eastern region of the CRB (Figure 5A). The Mesozoic volcanic rocks include basalts, andesites, spilites, and dolerites, or microgabbros of the Quebradagrande Complex [65,66,70], covering an area of 75.92 km² (i.e., 7.17%), and they are distributed from the central to the western region of the CRB (Figure 5A). The Cenozoic volcanic rocks correspond to lava domes and lava flows of the San Diego-Cerro Machín Volcano-Tectonic Province [44], covering an area of 154.88 km² (i.e., 14.63%), and they are located on the eastern side of the CRB (Figure 5A).

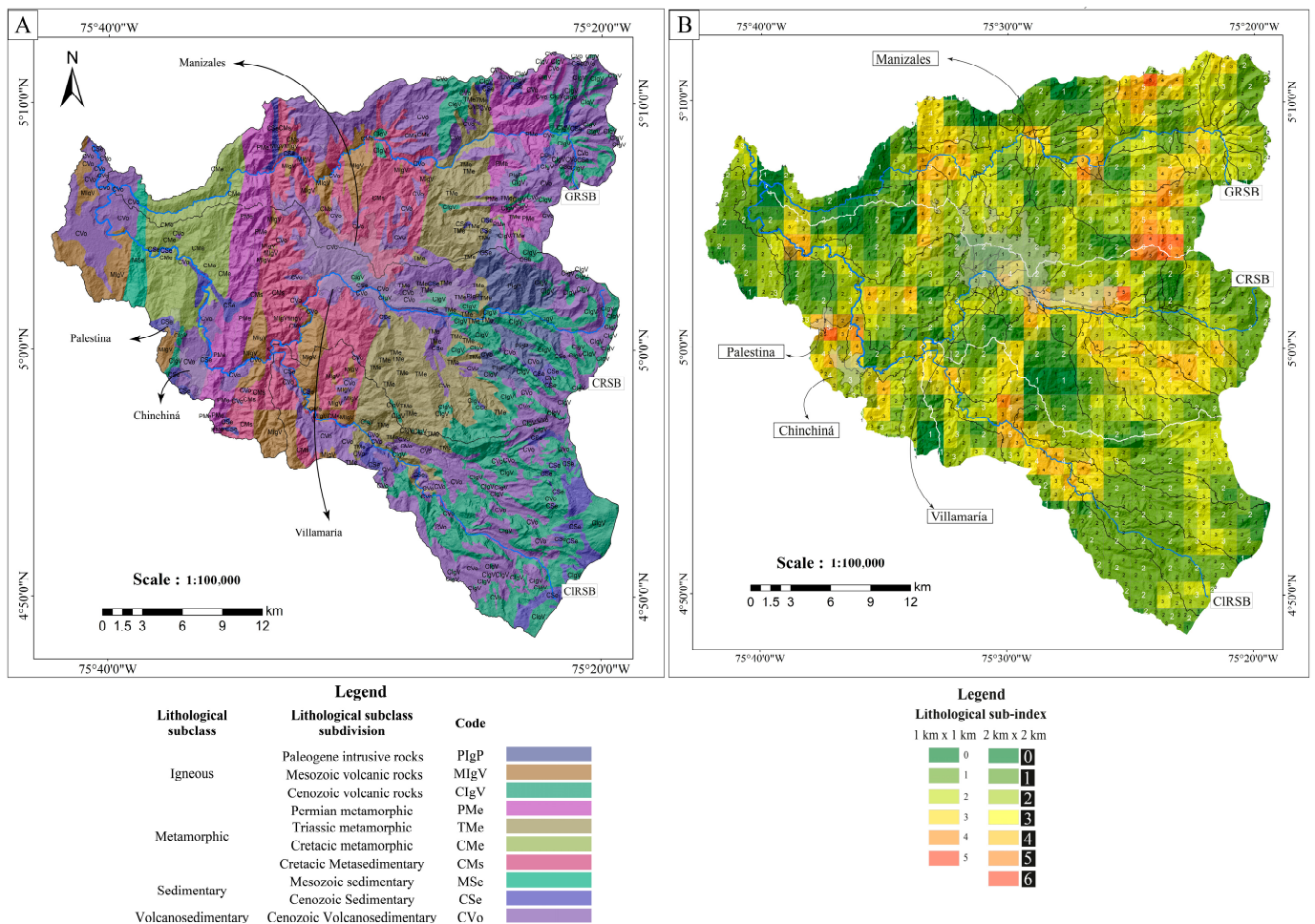


Figure 5. (A) Geological diversity of the Chinchiná River Basin. (B) Geological sub-index diversity of the Chinchiná River Basin.

- Metamorphic subclass

Permian metamorphic rocks correspond to migmatites, which have been described in the area as metamorphic granitoids [71,72], which are exposed throughout 84.60 km² (i.e., 7.99%) and located to the northeast of the Guacaica River Sub-Basin, as well as in the central-western region of the CRB (Figure 5A). Triassic metamorphic rocks include various lithologies with a low-to-medium degree of metamorphism, as well as greenschist-to-amphibolite facies, grouped in the Cajamarca Complex [65,66,73], covering an area of 117 km² (i.e., 11.05%), and they are located, from north to south, in the central-eastern region of the CRB (Figure 5A). Cretaceous metamorphic rocks correspond to garnet-bearing amphibolites, eclogites, and lawsonite-glaucophane-actinolite schist, as well as sedimentary or oceanic igneous protoliths, metagabbros and ultramafic rocks, and, occasionally, quartzites of the Arquia Complex [66,74,75], covering an area of 62.51 km² (i.e., 5.9%), and they are located in the western region of the CRB (Figure 5A). Metasedimentary rocks belong to the Quebradagrande Complex and include sandstones, black shales, feldspathic

sandstones, chert lenses, and limestones, which are affected by dynamic metamorphism, although they still preserve original sedimentary features [65,66,70,76]. They cover an area of 136.8 km² (i.e., 12.92%) and are located in the central region of the basin (Figure 5A).

- Sedimentary subclass

Mesozoic sedimentary rocks correspond to cherts, sandstones, and conglomerates of the Nogales Formation [77], covering an area of 9.77 km² (i.e., 0.92%), and they are in the western region of the CRB (Figure 5A). Cenozoic sedimentary deposits are composed of alluvial and glacial sediments, with the latter being made of volcanic lithics in a sandy–clay matrix [65,66], covering an area of 47.03 km² (i.e., 4.44%), and they are spread all over the basin (Figure 5A).

- Volcanosedimentary subclass

Volcanosedimentary deposits are related to different eruption periods, ranging from the Neogene period to the present, and include pyroclastic density currents, pyroclastic falls, debris avalanches, and lahars [43,48,49]; they cover an area of 323.27 km² (i.e., 30.54%) and are located all over the CRB (Figure 5A).

4.1.2. Geological Sub-Index of the Chinchiná River Basin

The geological sub-index of the CRB exposed how many abiotic lithological elements (i.e., types of rocks) converge per unit of territory (i.e., 1 km × 1 km and 2 km × 2 km geographical analyzed units) (Table 3). Generally, sites exhibiting the highest lithological diversity indices reveal two predominant patterns. The first, oriented in NE-SW directions, is situated in the western and central regions of the basin (Figure 5B), while the second is found in the southeastern region of the CRB, with two sets being oriented in a SE-NW direction (Figure 5B). Broadly, sectors exhibiting significant lithological diversity contain both ancient basement rocks and more recently formed geological formations.

Table 3. Areas and percentages of geological sub-index of the Chinchiná River Basin.

Lithological Elements	Area—%	Area—%
	1 km × 1 km Sub-Index	2 km × 2 km Sub-Index
1	195 km ² —18.6%	45 km ² —4.3%
2	538 km ² —51.5%	393 km ² —37.4%
3	265 km ² —25.2%	351 km ² —33.4%
4	50 km ² —18.6%	207 km ² —19.7%
5	3 km ² —0.30%	47 km ² —4.5%
6	0 km ² —0%	8 km ² —0.8%
Total	1051 km ² —100%	1051 km ² —100%

4.2. Geomorphology

4.2.1. Geomorphological Diversity of the Chinchiná River Basin

- Slope ranges subclass

The Central Cordillera’s mountainous terrain, where the CRB is situated, is distinguished by its steep inclines and varied slopes (Figure 6A). It comprises seven distinct slope ranges (Table 4).

- Landforms subclass

Broadly, the CRB features a rugged mountainous landscape, characterized by intricate, dissected slopes and a diverse array of volcanic and glacial landforms (Figure 6B). In total, 13 distinct geomorphological formations have been identified within the basin (Table 5).

- Drainage density subclass

The drainage density of the CRB was categorized into five groups, each representing a different abiotic element (Figure 6C) (Table 6).

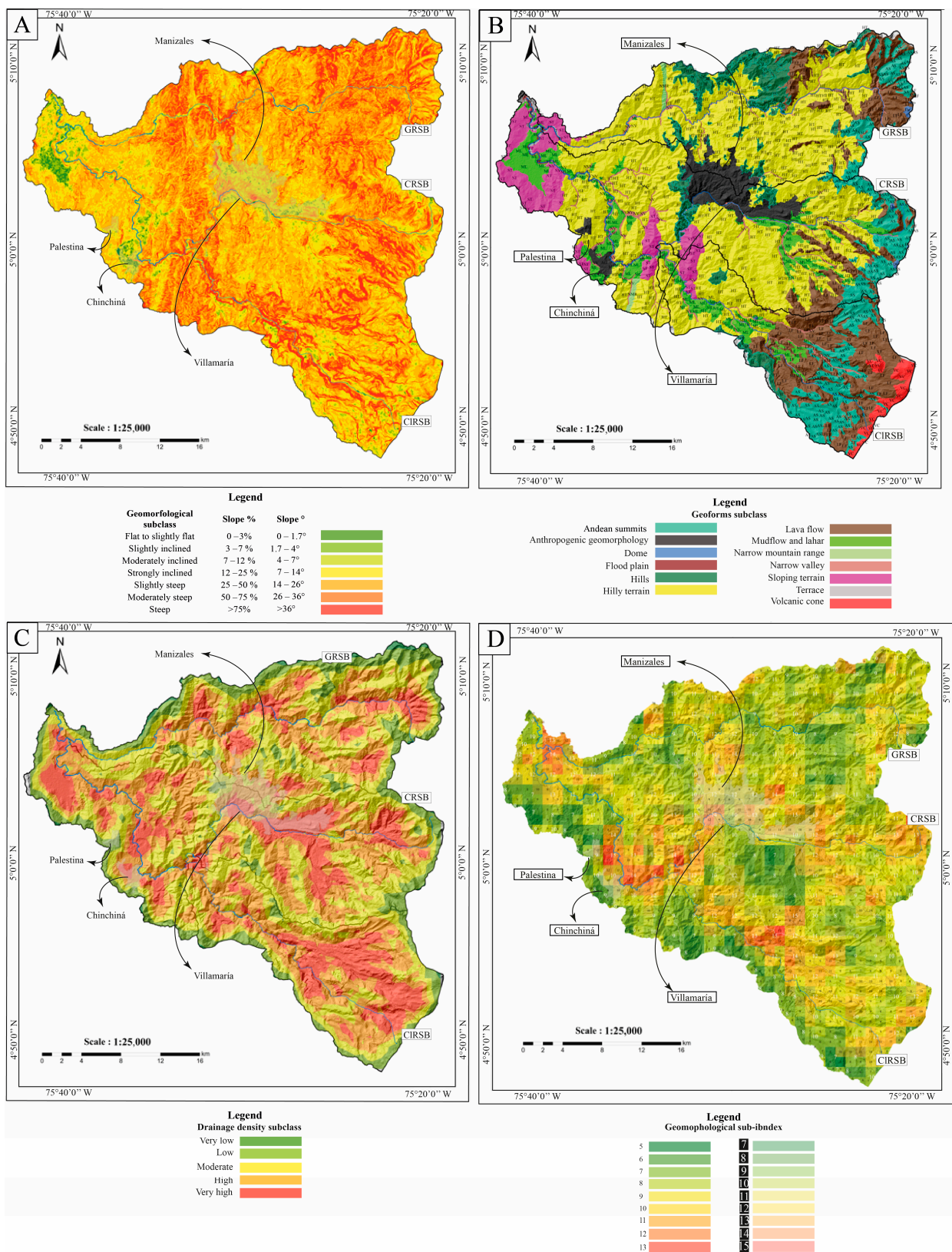


Figure 6. Geomorphological class. (A) Slopes range diversity of the Chinchiná River Basin. (B) Landform diversity of the Chinchiná River Basin. (C) Drainage Density of the Chinchiná River Basin. (D) Geomorphological sub-index of the Chinchiná River Basin. Cities are represented by different background colors.

Table 4. Geomorphological diversity of the Chinchiná River Basin.

Geomorphological Elements	Slope Ranges (%)	Slope Ranges (°)	Area—%
Flat-to-slightly flat slopes	0–3%	0°–1.7°	2 km ² —0.2%
Slightly inclined slopes	3–7%	1.7°–4°	8 km ² —0.8%
Moderately inclined slopes	7–12%	4°–7°	25 km ² —2.4%
Strongly inclined slopes	12–25%	7°–14°	189 km ² —18%
Slightly steep slopes	25–50%	14°–26°	500 km ² —47%
Moderately steep slopes	50–75%	26°–36°	231 km ² —22%
Steep slopes	>75%	>36°	96 km ² —9%
Total			1051 km ² —100%

Table 5. Geomorphologic units of the Chinchiná River Basin. Adapted from [67].

Landform	Description	Area—%
Andean summits	High mountain relief, including the Central Cordillera tallest peaks, which are typically associated with volcanoes. These summits exhibit glacial features.	105 km ² —10%
Anthropogenic geomorphology	Corresponds to the cities and towns within the basin, where an urban landscape prevails.	49 km ² —4.7%
Dome	Relief of lava material, with an approximately cylindrical base and slopes that range from very steep to subvertical.	1.5 km ² —0.1%
Flood plain	Constitutes the valley's lowest landform, aligning with the margins of the river's course and constantly receiving and depositing alluvial sediment from the riverbed.	2.3 km ² —0.2%
Hills	Corresponds to ancient volcanic–detritic deposits, being highly altered and moderately dissected and forming undulating and elongated units.	64 km ² —6.1%
Hilly terrain	These features exhibit the distinctive longitudinal and transverse forms found in mountain landscapes. The slopes are extended and straight and possess moderate-to-steep gradients.	478 km ² —45.1%
Lava flow	This relief is shaped by the accumulation of lava that descended from an emission center along the slope and subsequently solidified as it cooled.	166 km ² —15.8%
Mudflow and lahar	Corresponds to deposits originating from the high Andean peaks, resulting from a combination of volcanic, glacial, fluvial, and landslide processes. They settle in the middle and lower regions of the basin, obstructing valleys and forming extended terraces with generally gently sloping, flat-to-undulating surfaces.	70 km ² —6.7%
Narrow mountain range	It features a stepped pattern of triangular facets marked by uneven scarps, narrow sub-acute ridges, and straight slopes, with gradients ranging from steep to moderately steep, as well as exhibiting mild laminar erosion.	3.6 km ² —0.3%
Narrow valley	These are mountain tributaries that flow directly into the Cauca River. They primarily consist of alluvial formations, which are relatively small in size and typically exhibit elongated shapes with flat–concave topography. Their slopes are generally flat to gently inclined.	33.5 km ² —3.2%
Sloping terrain	These surfaces are linked to structural relief and defined by broad, smooth folds and gently tilted faulted layers.	59 km ² —5.6%
Terrace	This flat-to-slightly inclined relief is the outcome of two morphogenetic phases. Firstly, an accumulation phase, during which coarse and subsequently fine materials were deposited, occurred, followed by a phase of fluvial erosion, which shaped the slopes.	1.7 km ² —0.2%
Volcanic cone	This relief takes on a conical shape, featuring straight slopes with a concave appearance. The middle part of the slope is steep, though it gradually becomes gentler toward the base.	14.5 km ² —1.4%
Total		1051 km ² —100%

Table 6. Drainage density distribution of the Chinchiná River Basin.

Drainage Density	Area—%
Very low	5.6 km ² —0.6%
Low	120 km ² —11.5%
Moderate	328 km ² —31.3%
High	392 km ² —37.4%
Very high	202 km ² —19.2%
Total	1051 km ² —100%

4.2.2. Geomorphological Sub-Index of the Chinchiná River Basin

The geomorphological sub-index of the CRB exposed how many abiotic geomorphological elements (i.e., different slopes ranges, landforms, and drainage density) converge per unit of territory (i.e., 1 km × 1 km and 2 km × 2 km geographical analyzed units) (Table 7). There are three predominant patterns with the highest geomorphological index zones in the CRB, and they are primarily distributed in the central, southern, and southwestern regions of the basin (Figure 6B). In the northern region of the basin, moderate-to-high values of the index can be identified, yet it exhibits a lower level of diversity compared to those of the previously described areas (Figure 6B).

Table 7. Areas and percentages of the geomorphological sub-index of the Chinchiná River Basin.

Geomorphological Elements	Area—%	Area—%
	1 km × 1 km Sub-Index	2 km × 2 km Sub-Index
5	5 km ² —0.5%	-
6	78 km ² —7.4%	-
7	167 km ² —15.9%	35 km ² —3.3%
8	255 km ² —24.3%	82 km ² —7.8%
9	260 km ² —24.7%	134 km ² —12.7%
10	168 km ² —16%	252 km ² —24%
11	80 km ² —7.6%	211 km ² —20.1%
12	31 km ² —2.9%	223 km ² —21.2%
13	7 km ² —0.7%	65 km ² —6.2%
14	-	36 km ² —3.4%
15	-	13 km ² —1.2%
Total	1051 km ² —100%	1051 km ² —100%

4.3. Structural Geology

4.3.1. Structural Geological Diversity of the Chinchiná River Basin

The CRB features three predominant fault orientations (i.e., NS-NNE, NE-SW, and NW-SE) (Figure 7A). The faults exhibited distinct movements along both their horizontal (strike) and vertical (dip) axes; they were categorized by the function of the prevailing kinematic component (Table 8) (Figure 7A). Dextral faults include the Pico Terrible, La Cueva-Pirineo, and Cauca-Almaguer faults [43,78,79]. The dextral normal faults include the Santa-Rosa and El Perrillo faults [55,80,81]. The inistral faults include the Olleta-Nereidas, Nereidas, and Silvia-Pijao faults [43,82,83]. Reverse faults included the La Merced fault, as well as several lineaments and covered faults [55]. The reverse dextral faults include the Manizales-Aranzazu and Palestina faults [55,80]. The reverse sinistral fault corresponds to the El Perro fault [55]. The normal faults include the Rio Claro, Sancancio, and Cementerio-Solferino faults [55,84]. The normal sinistral fault corresponds to the Villamaría-Termale fault [55,80].

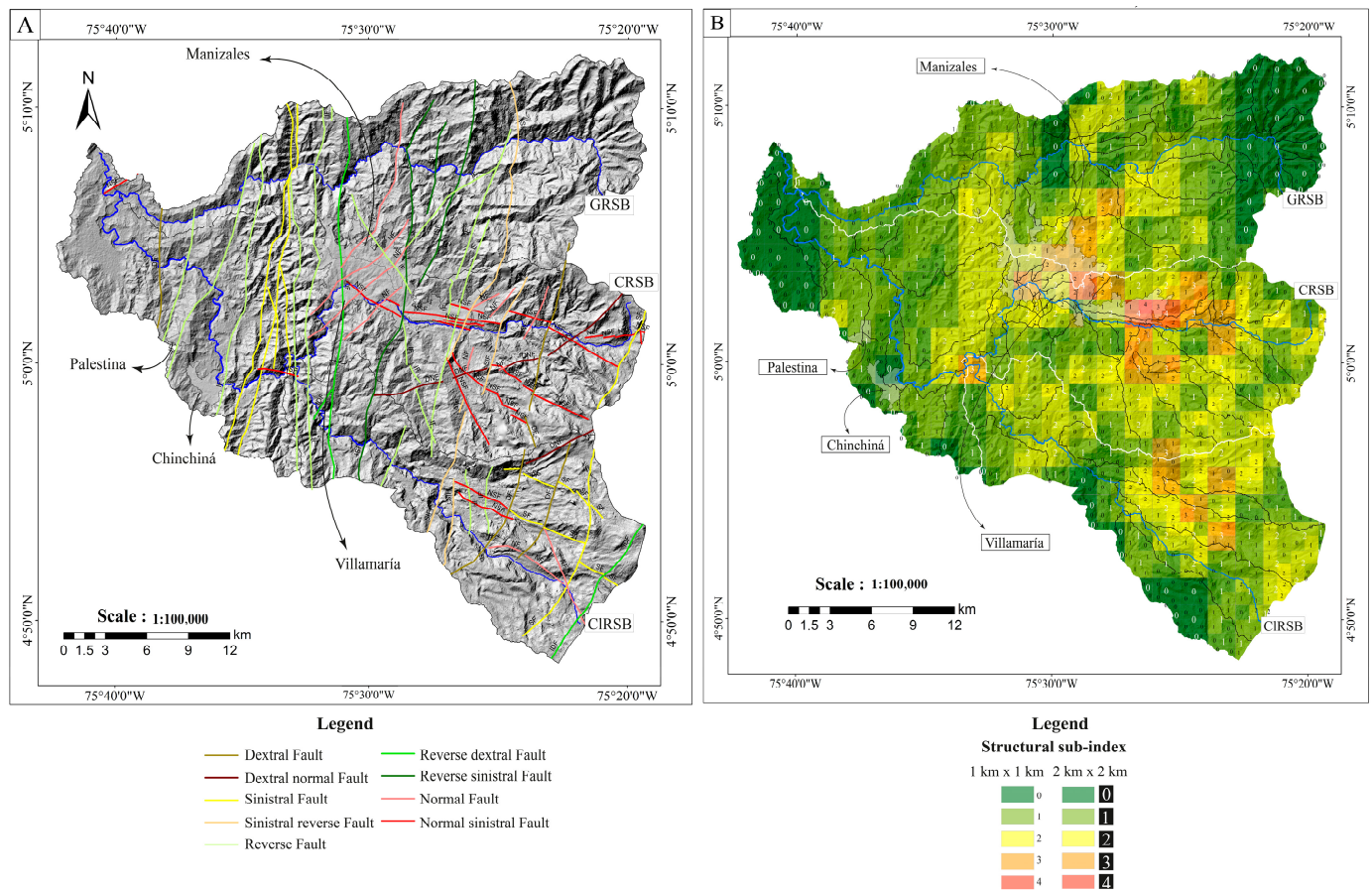


Figure 7. (A) Structural geological diversity of the Chinchiná River Basin. (B) Structural geological sub-index diversity of the Chinchiná River Basin.

Table 8. Structural subclasses and abiotic elements.

Structural Geology Subclass	Abiotic Structural Elements	Fault Length—%
Dextral	Dextral faults	42.6 km—7%
	Dextral normal faults	22.4 km—3.7%
Sinistral	Sinistral faults	104 km—17%
	Sinistral reverse faults	47 km—7.7%
Reverse	Reverse faults	171 km—28%
	Reverse dextral faults	40.4 km—6.6%
Normal	Reverse sinistral fault	50 km—8.2%
	Normal faults	63 km—10.3%
	Normal sinistral faults	70 km—11.5%
	Total	610.4 km—100%

4.3.2. Structural Geological Sub-Index of the Chinchiná River Basin

The structural geological sub-index of the CRB exposed how many abiotic fault tendencies converge per unit of territory (i.e., 1 km × 1 km and 2 km × 2 km geographical analyzed units) (Table 9). Generally, the areas with the highest sub-index values could be categorized into three groups: (1) the first, situated at the center of the CRB, encompassing the towns of Manizales and Villamaría, with a predominant NE-SW trend; (2) the second, in comparison with previous trend, is located eastward, within the central-eastern region of the CRB, and maintains the NE-SW trend; and (3) the third is positioned in the southeastern region of the basin (Figure 7B). It is noteworthy that the highest values of the structural geological sub-index are adjacent to the urban areas of Manizales and Villamaría (Figure 7B).

Table 9. Areas and percentages of structural sub-index in the Chinchiná River Basin.

Structural Geological Elements	Area—%	
	1 km × 1 km Sub-Index	2 km × 2 km Sub-Index
0	402 km ² —38.2%	158 km ² —12%
1	522 km ² —49.7%	462 km ² —44%
2	112 km ² —10.7%	343 km ² —32.6%
3	14 km ² —1.3%	76 km ² —7.2%
4	1 km ² —0.1%	12 km ² —1.1%
Total	1051 km ² —100%	1051 km ² —100%

4.4. Pedology

4.4.1. Pedological Diversity of the Chinchiná River Basin

The seven categories comprising the pedological diversity of the CRB are constituted by (1) Andisols, which are common in areas where volcanic and volcanoclastic materials are present [85], occupy 658 km² (i.e., 62.8%) of the basin, and are distributed over the eastern-central region of the CRB (Figure 8A); (2) Inceptisols, which, except for arid locations, can occur in almost any environment [85], occupy 26 km² (i.e., 2.5%) of the basin, and are located over active landscapes throughout the river channels (Figure 8A); (3) Mollisols, which form either on grasslands in climates with moderate-to-pronounced seasonal moisture deficit, under forest ecosystems, on marshes, or on loams in humid climates [85], occupy 217 km² (i.e., 20.7%) of the basin, and are distributed from the central to the western regions of the CRB (Figure 8A); (4) Histosols, which generally consist of decomposed plant remains that accumulated in water, are freely drained and known as peats [85], cover 1 km² (i.e., 0.1%) of the basin, and can be found as fragmented islands through the eastern and southeastern regions of the CRB (Figure 8A); (5) Entisols, which are characteristic of active areas (e.g., steep eroding slopes, flood plains or glacial plains) [85], occupy 33 km² (i.e., 3.2%) of the basin, and are distributed over river channels where not enough soil material exists for pedogenic processes to take place (Figure 8A); (6) No soil formation, which corresponds to places where climatic (e.g., highest summits of the basin) or topographic (e.g., escarpments) conditions limit soil formation processes and vegetative development [67], occupies 64 km² (i.e., 6.1%), and are located in the southeastern-most region of the CRB (Figure 8A); and (7) Anthropogenic soil, which corresponds to the areas where urban dynamics take place and concrete and metal structures drive transcendental changes over the soil and occupies 49 km² (i.e., 5%) of the basin (Figure 8A).

4.4.2. Pedological Sub-Index of the Chinchiná River Basin

The pedological sub-index of the CRB exposed how many pedological elements (i.e., different soil orders/categories) converge per unit of territory (i.e., 1 km × 1 km and 2 km × 2 km geographical analyzed units) (Table 10). The index generally rises from east to west, with the highest values concentrated in the area between the urban centers of Manizales, Chinchiná, and Palestina in the southwestern region of the CRB. Additionally, notable high indices can also be observed to the north and west of Manizales (Figure 8B).

Table 10. Areas and percentages of the pedological sub-index in the Chinchiná River Basin.

Pedological Elements	Area—%	
	1 km × 1 km Sub-Index	2 km × 2 km Sub-Index
1	394 km ² —37%	168 km ² —16%
2	417 km ² —40%	377 km ² —36%
3	172 km ² —16%	311 km ² —30%
4	59 km ² —6%	163 km ² —16%
5	9 km ² —1%	32 km ² —3%
Total	1051 km ² —100%	1051 km ² —100%

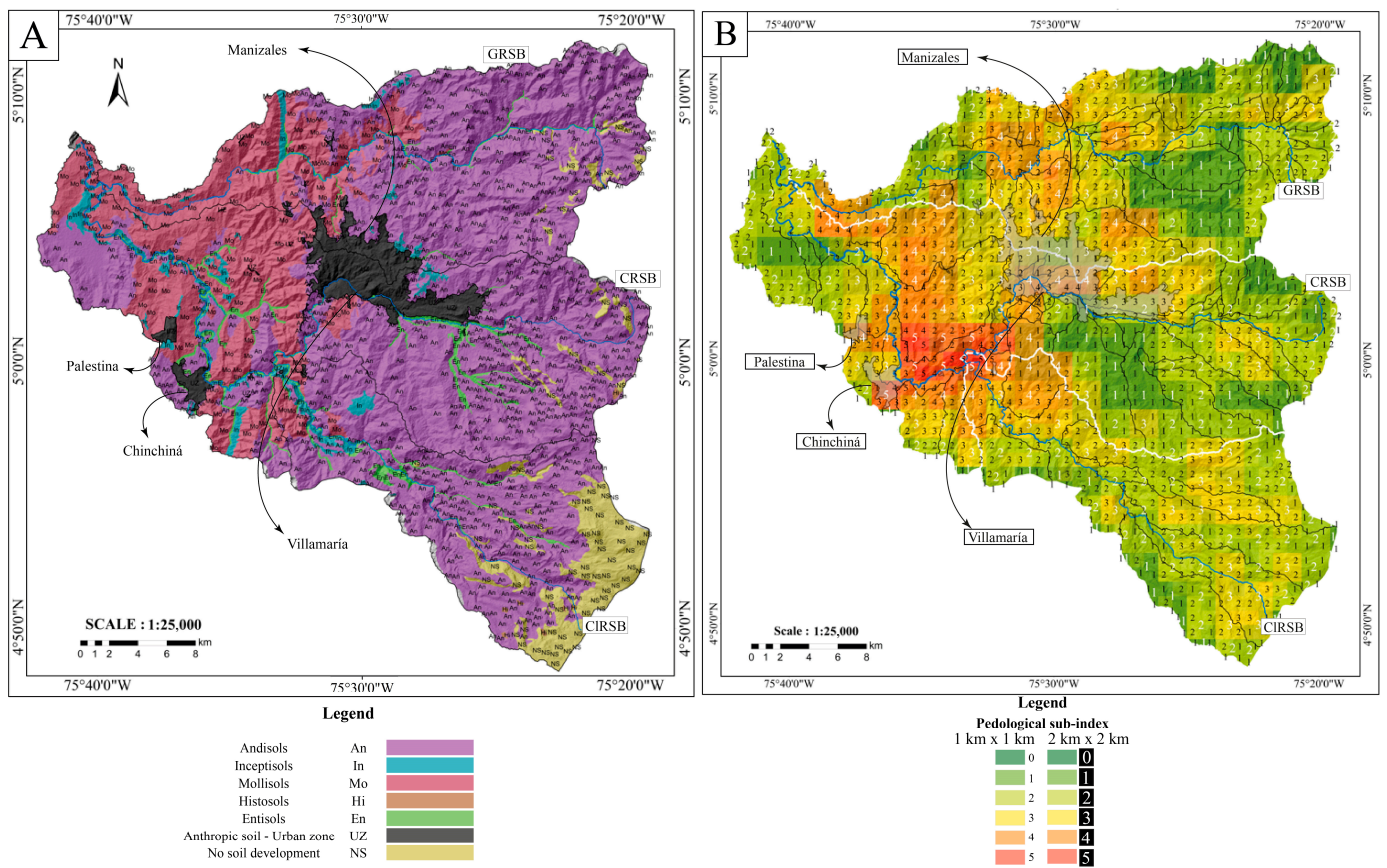


Figure 8. (A) Pedological diversity of the Chinchiná River Basin. (B) Pedological sub-index diversity of the Chinchiná River Basin. Cities are represented by different background colors.

4.5. Climatology

4.5.1. Climatological Diversity of the Chinchiná River Basin

- Snow

The snow climate is in the highest region of the CRB, i.e., over 4200 m.a.s.l., covering 48.5 km² (i.e., 4.6%) in the southeastern region of the basin (Figure 9A). The abiotic climatic element (i.e., perpetual snow) is characterized by subnival and nival thermal floors, with temperatures ranging from 0 °C to 3 °C [61] (Figure 9A).

- Paramo

The paramo climate is distributed throughout 276.7 km² (i.e., 26.3%) beneath the permanent snow cover, ranging from south to north in the eastern perimeter of the CRB (Figure 9A). It is composed of three sub-climates: (1) the superhumid high paramo, with temperature varying from 3 °C to 7 °C and precipitation varying between 125 and 500 mm per year [61], is spread over 78 km² (i.e., 7%); (2) the superhumid low paramo, with temperatures ranging from 7 °C to 12 °C and precipitation of 500–1000 mm per year [61], is spread over 178.7 km² (i.e., 17%); and (3) the low humid paramo, with temperatures ranging from 7 °C to 12 °C and precipitation of 250–500 mm per year [61], is spread over 19.7 km² (i.e., 2%) of the basin (Figure 9A).

- Cold

The cold climate, situated between 2000 and 3000 m. a. s. l., with temperatures ranging from 12 °C to 17 °C [61], is distributed over 366 km² (i.e., 34.8%) of the basin, beneath the paramo climate (Figure 9A). It is composed of three sub-climates: (1) the superhumid cold climate, with precipitation of 2000–4000 mm per year [61], is distributed over 9.2 km² (i.e., 1%); (2) the cold wet climate, with precipitation of 1000–2000 mm per year [61], is

distributed over 341 km² (i.e., 32.4%); and (3) the cold semi-humid, with precipitation of 500–1000 mm per year [61], is distributed over 16.2 km² (i.e., 1.5%) of the basin (Figure 9A).

- Temperate

The temperate climate is distributed from the center to the west of the basin, between 1000 and 2000 m. a. s. l., with temperatures ranging from 18 °C to 24 °C [61], and it is distributed over 339 km² (i.e., 32%) beneath the cold climate (Figure 9A). It is composed of two sub-climates: (1) the moist temperate climate, with average precipitation of 2000–4000 mm per year [61], is distributed over 309.7 km² (i.e., 29%), and (2) the semi-humid temperate climate, with precipitation of 1000–2000 mm per year [61], is distributed over 29 km² (i.e., 2.7%) of the basin (Figure 9A).

- Warm

The warm climate is in the westernmost area of the CRB, at between 800 and 1000 m. a. s. l., with temperatures >24 °C [61], and it covers over 22 km² (2%) of the basin (Figure 9A). It is composed of two sub-climates: (1) the warm-humid climate, with precipitation of 4000–8000 mm per year [61], is distributed over 0.5 km² (i.e., 0.05%), and (2) the warm semi-humid climate, with precipitation of 2000–4000 mm per year [61], is distributed over 21.5 km² (i.e., 2%) (Figure 9A).

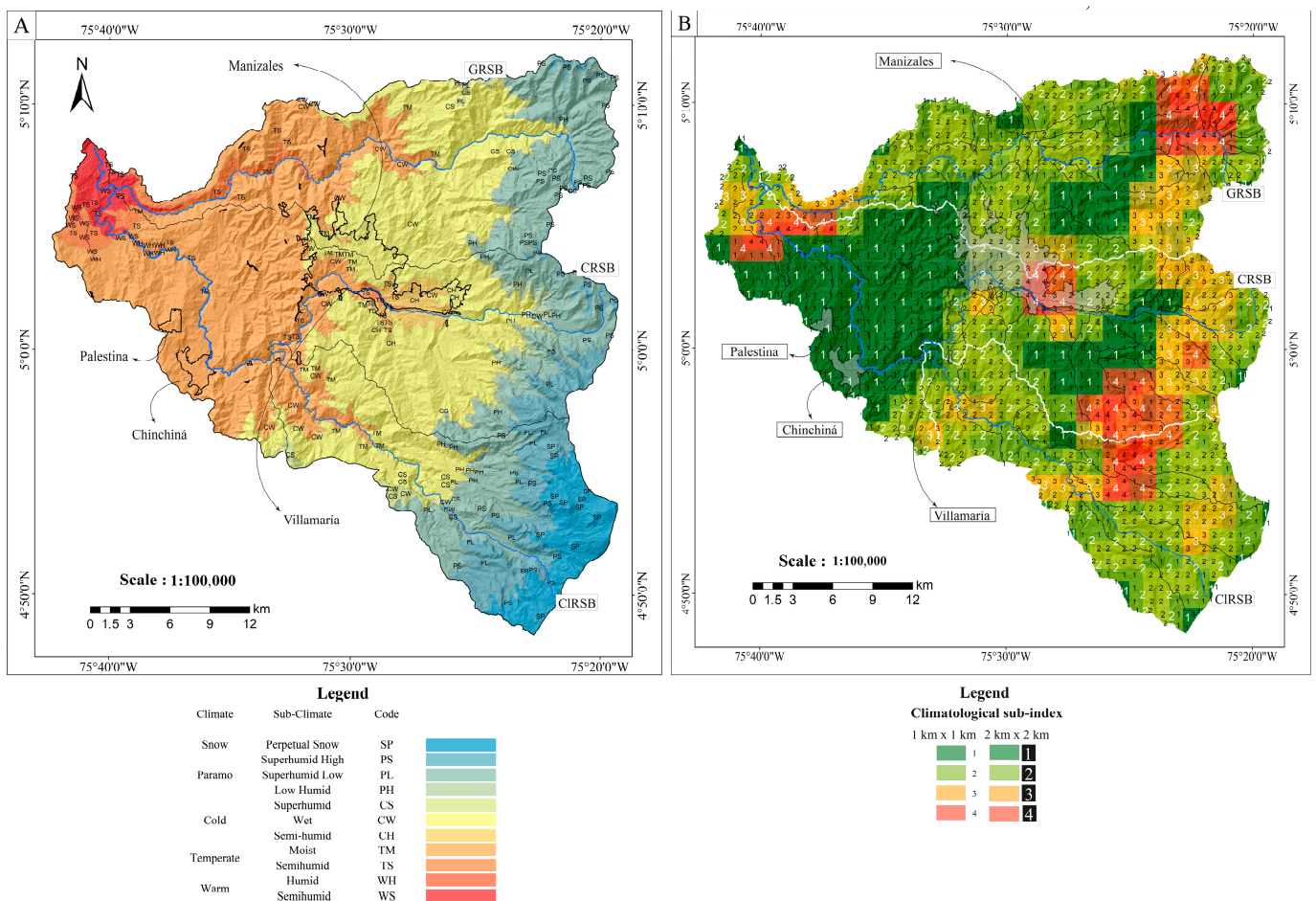


Figure 9. (A) Climatological diversity of the Chinchiná River Basin. (B) Climatological sub-index diversity of the Chinchiná River Basin.

4.5.2. Climatological Sub-Index of the Chinchiná River Basin

The climatological sub-index of the CRB exposed how many different types of climates converge per unit of territory (i.e., 1 km × 1 km and 2 km × 2 km geographically analyzed

units) (Table 11). Generally, the CRB exhibits four sectors with high climatological diversity indices (Figure 9B). Two of these sectors are situated in the high mountain area in the eastern region of the basin, connected to another sector with high climatological diversity (Figure 9B). Another sector with a high climatological sub-index is found in the Manizales-Villamaría area, and the final one is situated in the western-most region of the basin (Figure 9B).

Table 11. Areas and percentages of climatological sub-index of the Chinchiná River Basin.

Climatological Elements	Area—%	
	1 km × 1 km Sub-Index	2 km × 2 km Sub-Index
1	537 km ² —51.1%	275 km ² —26.2%
2	399 km ² —38%	495 km ² —47.1%
3	72 km ² —6.9%	157 km ² —14.9%
4	43 km ² —4.1%	124 km ² —11.8%
Total	1051 km ² —100%	1051 km ² —100%

4.6. Hydrology

4.6.1. Hydrological Diversity of the Chinchiná River Basin

The seven stream orders comprising the CRB water net surface drainage represent a total of 3329 km; the main rivers with the highest orders are located downstream, in the western region of the basin, where all the tributaries converge and eventually flow into the Cauca River (Figure 10A). In the western region of the CRB is the “Santagueda—km 41” aquifer, corresponding to a multilayered aquifer with primary porosity and both free and semiconfined levels [86] (Figure 10A). In the eastern/southeastern region, three sectors small lakes can be found, some of which are derived from glacier retreat processes, and others are products of paramo wetlands (Figure 10A). In the highest sectors of the basin, two of the six remaining glaciers of Colombia are located at the summits of the Nevado del Ruiz and Nevado Santa Isabel volcanoes (Figure 10A).

4.6.2. Hydrological Sub-Index of the Chinchiná River Basin

The hydrological sub-index of the CRB represents how many hydrological elements (i.e., stream orders + aquifers + lakes + glaciers) converge per unit of territory (i.e., 1 km × 1 km and 2 km × 2 km geographical analyzed units) (Table 12). The hydrological sub-index generally increases in an east–west direction, particularly over the main river channels, which correspond to the highest indices (Figure 10B). Notably, in the western region, where the highest drainage order is situated, the highest indices align with the presence of the basin’s groundwater aquifer (Figure 10B). In the southeastern region, where the lakes and glaciers are located, a slight increase in the index can be observed (Figure 10B). Conversely, lower values are observed in the upper and middle regions of the CRB, where smaller tributaries originating from hill summits flow into the valleys and contribute to the main rivers (Figure 10B).

Table 12. Areas and percentages of hydrological sub-index of the Chinchiná River Basin.

Hydrological Elements	Area—%	
	1 km × 1 km Sub-Index	2 km × 2 km Sub-Index
1	255 km ² —24.3%	63 km ² —6%
2	529 km ² —50.4%	516 km ² —49.1%
3	213 km ² —20.3%	371 km ² —35.3%
4	30 km ² —2.9%	64 km ² —6.1%
5	23 km ² —2.2%	37 km ² —3.5%
Total	1051 km ² —100%	1051 km ² —100%

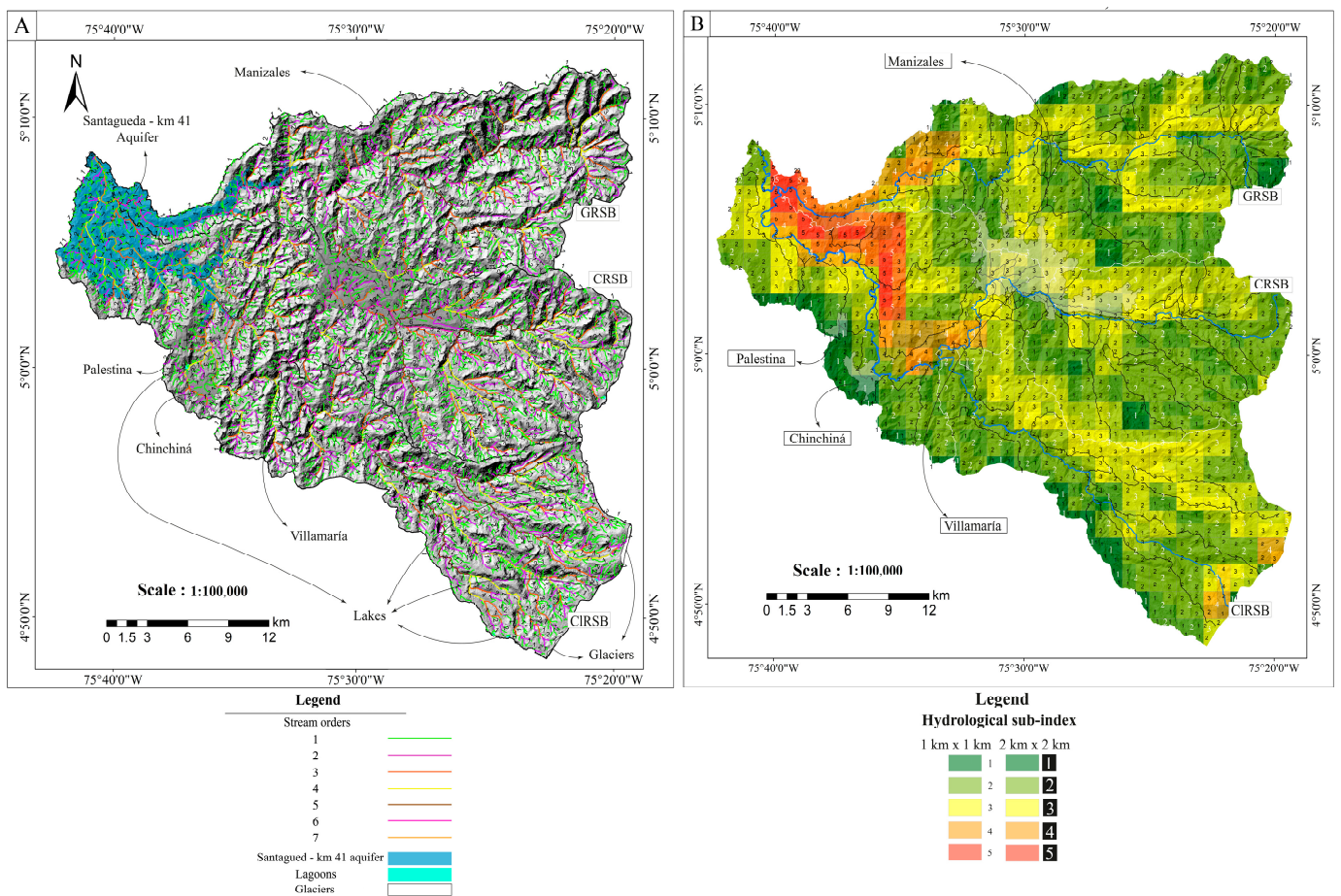


Figure 10. (A) Hydrological diversity of the Chinchiná River Basin. **(B)** Hydrological sub-index diversity of the Chinchiná River Basin.

4.7. Volcanology

4.7.1. Volcanological Diversity of the Chinchiná River Basin

The two categories comprising volcanological diversity in the CRB are made up of 5 polygenetic and 22 monogenetic volcanoes (Figure 11A). Polygenetic volcanoes are predominantly situated in the southeastern region of the basin, with only one located in the northeastern region (Figure 11A). Conversely, monogenetic volcanoes are primarily distributed in the central region of the basin, where the Villamaría-Termales monogenetic volcanic field is located [46,47], as well as in the northern region of the basin, where the Tapias-Guacaica monogenetic volcanic field is located [51–53] (Figure 11A).

4.7.2. Volcanological Sub-Index of the Chinchiná River Basin

The volcanological sub-index of the CRB represents the volcanoes converging per unit of territory (i.e., 1 km × 1 km and 2 km × 2 km geographical analyzed units) (Table 13). Four significant volcanological high-indices areas are distributed across the basin (Figure 11A). To the southeast, there are polygenetic volcanoes influencing high values, while in the central, central-eastern, and northern regions, monogenetic volcanoes are responsible for high sub-indices values (Figure 11A).

Table 13. Areas and percentages of the volcanological sub-index in the Chinchiná River Basin.

Volcanological Elements	Area—%	Area—%
	1 km × 1 km Sub-Index	2 km × 2 km Sub-Index
0	967 km ² —91.1%	917 km ² —87.2%
1	87 km ² —8.3%	105 km ² —10%
2	7 km ² —0.7%	21.7 km ² —2.1%
3	-	7.5 km ² —0.7%
Total	1051 km ² —100%	1051 km ² —100%

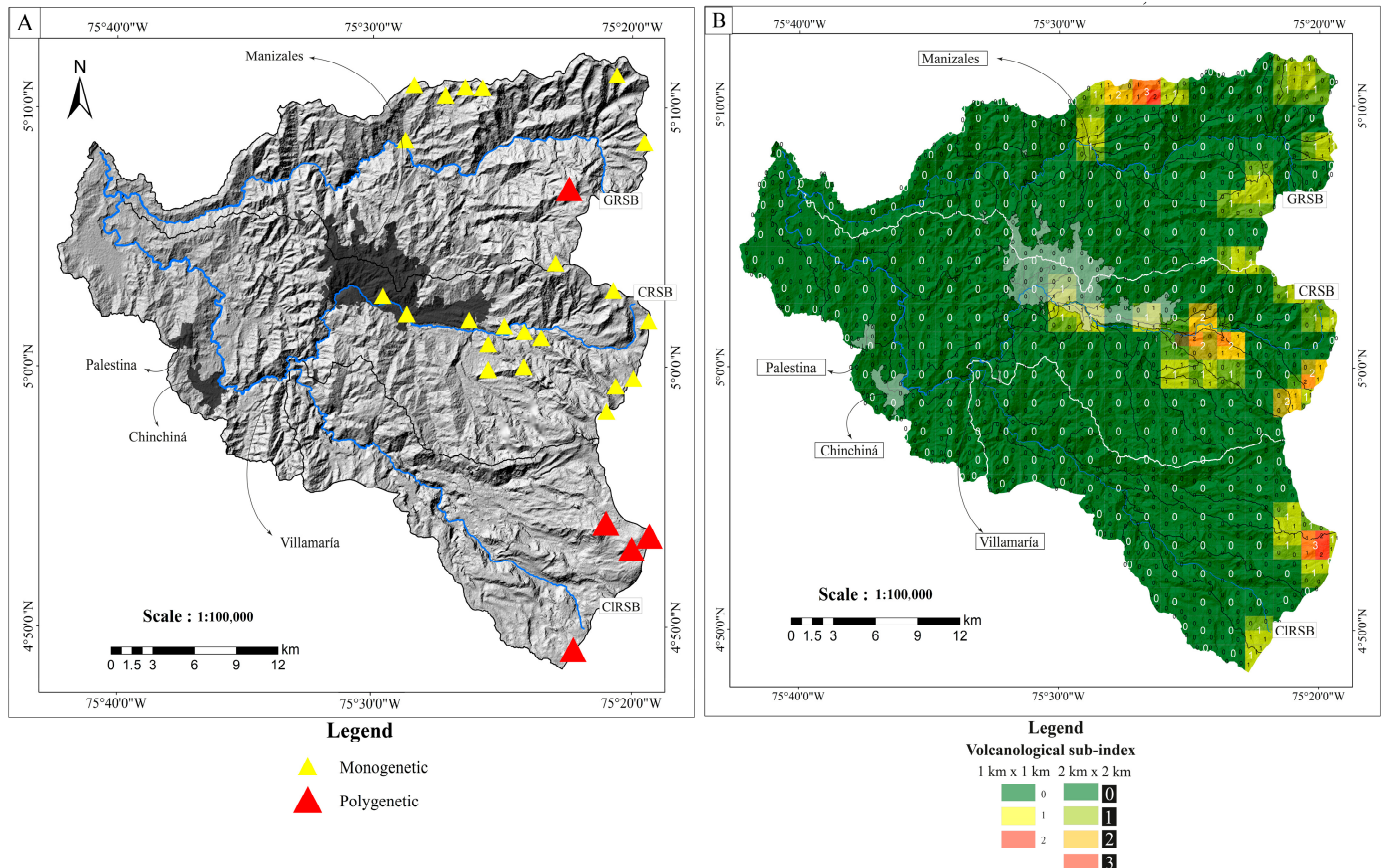


Figure 11. (A) Volcanological diversity of the Chinchiná River Basin. (B) Volcanological sub-index diversity of the Chinchiná River Basin. Cities represented by different background colors.

4.8. Geothermal

4.8.1. Geothermal Diversity of the Chinchiná River Basin

The three categories comprising the geothermal diversity of the CRB are constituted by 3 hot spring manifestations below 35 °C, 11 hot springs between 35 °C and 70 °C, and 2 hot springs over 70 °C (Figure 12A). Most of the CRB hot springs occur in the southern region in the Claro River Sub-Basin toward its center and over the main course of the river; otherwise, a few other hot springs are located to the southeast of the Chinchiná River Sub-Basin (Figure 12A).

4.8.2. Geothermal Sub-Index of the Chinchiná River Basin

The geothermal sub-index of the CRB represents how many temperature ranges converge per unit of territory (i.e., 1 km × 1 km and 2 km × 2 km geographical analyzed units) (Table 14). Overall, the geothermal sub-index predominantly exhibits values in the south-southeastern region of the CRB, with the majority of these values concentrated within the Claro River Sub-Basin (Figure 12B). Notably, a significant area of geothermal diversity

is observed in the central-middle region of the Claro River Sub-Basin, where three distinct temperature ranges converge within the analyzed 2 km × 2 km sub-index (Figure 12B).

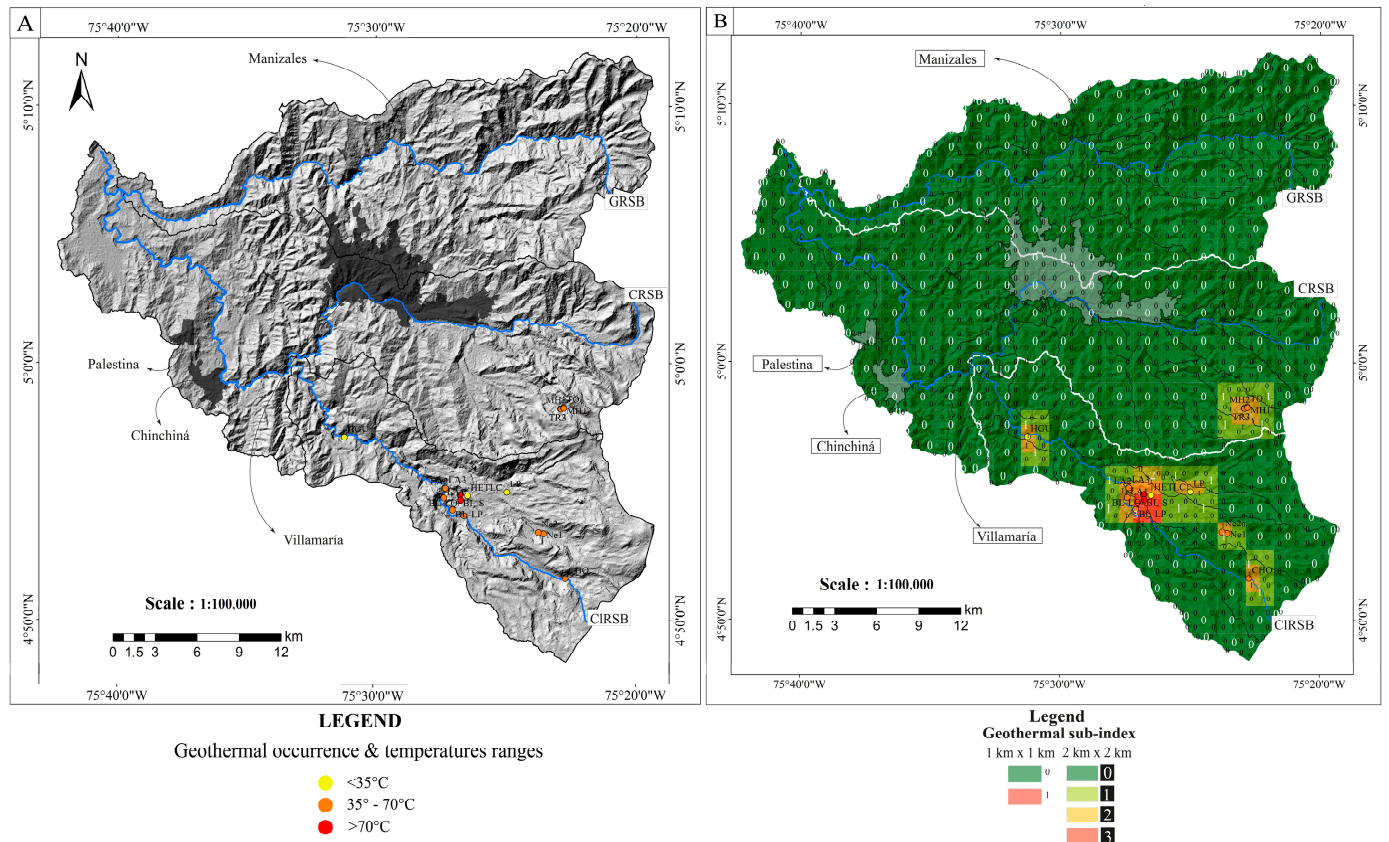


Figure 12. (A) Geothermal diversity of the Chinchiná River Basin. (B) Geothermal sub-index diversity of the Chinchiná River Basin. Cities represented by different background colors.

Table 14. Areas and percentages of the geothermal sub-index in the Chinchiná River Basin.

Geothermal Elements	Area—%	Area—%
	1 km × 1 km Sub-Index	2 km × 2 km Sub-Index
0	1031 km ² —98%	983 km ² —93.5%
1	20 km ² —2%	60 km ² —5.7%
2	-	4 km ² —0.4%
3	-	4 km ² —0.4%
Total	1051 km ² —100%	1051 km ² —100%

4.9. General Geodiversity Index

Two results of geodiversity quantification are presented: (1) the total count of abiotic elements and (2) the statistical weighting of the sub-indices (Figure 13). Both maps reveal a consistent trend and highlight areas within the basin with the highest and lowest abiotic diversity. Both the south-southeastern and central-eastern regions exhibit clusters of high geodiversity. Notably, the highest index values are concentrated near the main riverbeds of the Claro and Chinchiná rivers. Another region with a notably high geodiversity index is found in the north-central region within the Guacaica River Sub-Basin. Conversely, regions with lower abiotic diversity values are identifiable, being primarily located in the southern and north-eastern regions of the Manizales-Villamaría urban center in the Chinchiná River Sub-Basin, as well as in the western region of the basin.

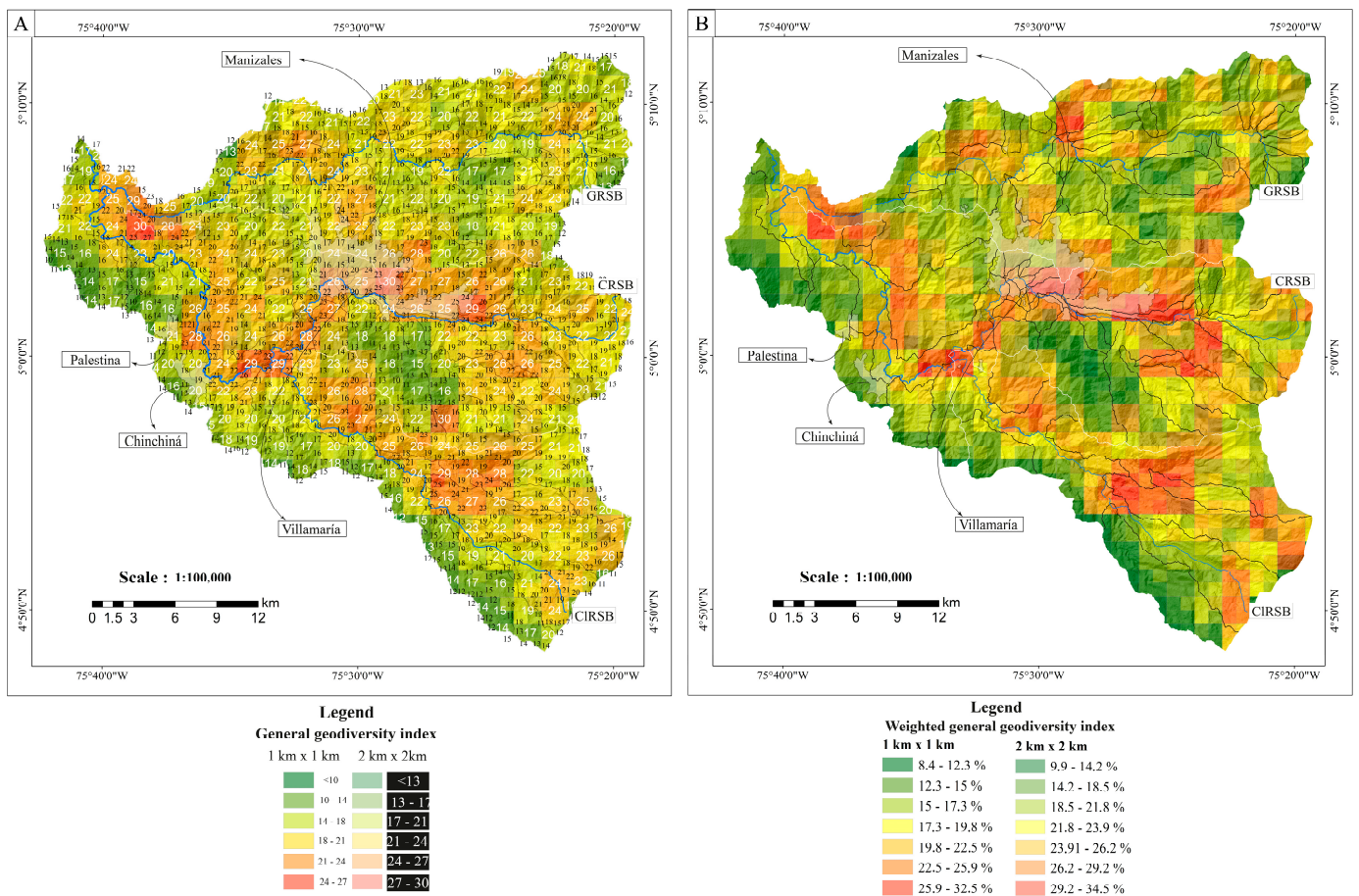


Figure 13. (A) General geodiversity index from the sum of geodiversity sub-indices; (B) general geodiversity index after the statistical weighting of classes.

It is noteworthy to compare both results: the first provides the total number of abiotic elements per geographical unit of analysis (Table 15), while the second (Table 2) indicates the percentage of geodiversity per geographical unit of analysis. Among the 105 abiotic elements analyzed, up to 27 can converge within a 1 km × 1 km geographical analyzed unit, while up to 30 can converge within 2 km × 2 km units. The first figure represents around 32.5% of the geodiversity that can be observed in 1 km × 1 km units, while the latter figure represents around 34.5% that can be found in 2 km × 2 km areas.

Table 15. General geodiversity index percentages for geographically analyzed units (i.e., 1 km × 1 km and 2 km × 2 km).

General Geodiversity Index	Area—%	
	1 km × 1 km Sub-Index	2 km × 2 km Sub-Index
10	4 km ² —0.4%	-
11	14 km ² —1.3%	-
12	28 km ² —2.7%	-
13	47 km ² —4.5%	2 km ² —%
14	94 km ² —8.9%	9 km ² —%
15	138 km ² —13.1%	22 km ² —%
16	127 km ² —12.1%	28 km ² —%
17	112 km ² —10.7%	42 km ² —%
18	134 km ² —12.7%	30 km ² —%
19	118 km ² —11.2%	36 km ² —%
20	70 km ² —6.7%	108 km ² —%

Table 15. Cont.

General Geodiversity Index	Area—%	
	1 km × 1 km Sub-Index	2 km × 2 km Sub-Index
21	68 km ² —6.5%	136 km ² —%
22	50 km ² —4.8%	151 km ² —%
23	21 km ² —2%	114 km ² —%
24	16 km ² —1.5%	130 km ² —%
25	7 km ² —0.7%	66 km ² —%
26	2 km ² —0.2%	84 km ² —%
27	1 km ² —0.1%	28 km ² —%
28	-	32 km ² —%
29	-	19 km ² —%
30	-	12 km ² —%
Total	1051 km ² —100%	1051 km ² —100%

5. Discussion

5.1. Methodological Constraints

When studying geodiversity, various factors, such as research objectives, cartographic information quality, study scale, geodiversity classes classification criteria, grid size for territorial segmentation, and data processing equipment influence the chosen methodology, which, in turn, plays a pivotal role in shaping the resulting outcomes [2,14,25]. The more aspects considered for geodiversity estimation, the more enhanced the study's comprehensiveness, but an increasing number of variables require more class definitions and information management, resulting in greater study complexity [2]. In fact, there are many examples of geodiversity quantification in which some abiotic elements are omitted [15,17,20,26]. This does not necessarily mean that the result is wrong, simply showing that their context of development is limited by a framework that depends on the conditions of the method previously shown [3,16,21,23–25].

5.1.1. Quality and Scale of Information

When examining the number of abiotic elements and the associated sub-index values across different classes, notable disparities become apparent. Some classes encompass a more extensive range of subclasses, whereas others not only have fewer abiotic elements but also show lower values in the sub-indices. According to the multivariate methodology used in this study, places with higher numbers of abiotic elements are more geodiverse than places with a lower number of abiotic elements. Hence, classes with higher numbers of abiotic elements exert a more significant influence on the final geodiversity result.

It is important to note that the geodiversity index calculated for the CRB includes two classes (i.e., geomorphological and pedological) with cartographic information at a more detailed scale (i.e., 1:25,000), in contrast to the other geodiversity classes (i.e., 1:100,000). It is, therefore, crucial to assess how these variations in scale impact both indices and their contributions to the final geodiversity result.

In the case of the pedological class, seven distinct abiotic elements were identified (Figure 8A). When extending these observations into quantitative analyses, it can be observed that the maximum sub-index value corresponds to five abiotic pedological elements per unit of territory (Table 10). In terms of abundance, both calculated indices show that it is most common to find two soil types per unit of territory (Table 10). Interestingly, compared to other geodiversity classes, where the base cartographic information is at a less detailed scale (e.g., rocks, faults, climate, water), it becomes evident that there are no significant disparities between the indices, and their maximum values exhibit similar trends (Tables 3, 9 and 11). Conversely, a notable difference becomes apparent when analyzing the geomorphological class. The disparity in both the quantity of abiotic elements and the corresponding subindex calculated for this class is evident when making comparisons with to the other geodiversity classes (Table 7). While the scale factor certainly contributes to

this variation, it is equally crucial to underscore the composition of the subclasses used for geomorphological analysis (i.e., slopes, landforms, and drainage density). These subclasses encompass abiotic elements distributed throughout the entire basin, in contrast to other geodiversity classes, in which extensive areas lack abiotic elements (e.g., volcanoes, faults, hot springs). This distinction underscores, on one hand, the substantial impact of the geomorphological class on the geodiversity index due to the scale of its base cartographic information. On the other hand, it reflects the intrinsic characteristics of the basin, shaped by its intricate topographic diversity and the range of reliefs arising from the mountainous and orogenic environment in which the CRB is situated.

5.1.2. Weighting of Classes

In pursuit of a more robust comparative analysis among classes and in response to the scale-related limitations identified, we introduced a statistical processing approach for subindexes and classes. Our objective was to provide a more detailed interpretation of the significance of each geographical unit of analysis within the context of the total geodiversity of the basin. To achieve this goal, we calculated the relative percentage of each subindex in relation to the total abiotic elements within each class (Table 2). Subsequently, we assigned a weight to each subindex, corresponding to the equivalent percentage assigned to each class. Specifically, with eight classes in total, each class has attributed a value of 12.5%, since we did not establish value criteria that gave greater or lesser importance to one class over another class.

This method allowed us to address the disparities observed in the geomorphology class resulting from the cumulative count of abiotic elements, which was influenced by scale-related issues. Therefore, an equivalent percentage subindex was derived for each class, contingent on both the total abiotic elements within each class and the total subclasses considered in the geodiversity calculation (Table 2). Consequently, the outcome reveals distinct weights assigned to the classes for each geographical unit of analysis, contingent upon the input parameters unique to each class (Table 2).

The geographical pattern illustrated on the map with the weighted sub-index is aligned with the initial trend derived from the summation of abiotic elements (Figure 13). This alignment affirms the reliability and applicability of the generated map. However, it introduces a significant shift in how values are interpreted. Instead of focusing on the quantity of abiotic elements, it now represents the percentage of total geodiversity per geographical unit of analysis. This result is interesting when comparing areas for which geodiversity indices are calculated.

5.1.3. Influence of Grid Size

It is indeed important to acknowledge the influence of grid size on the quantification of the geodiversity index because it can significantly impact the number of geodiversity elements included per unit of territory, subsequently modifying the calculated value of the index [87,88]. This was evident in the study's analysis, as two different grid sizes (i.e., 1 km × 1 km and 2 km × 2 km) were used to calculate the sub-indices. Notably, when using a larger grid size, more geodiversity elements tended to be encompassed within each grid, potentially resulting in a higher geodiversity index value. Conversely, employing a smaller grid size reduced the number of elements accounted for per unit of territory, which could lower the index value. The larger the difference between the analysis grid sizes used, the greater the disparity between the resulting sub-indices and, possibly, the differences in the number and distribution of geodiversity elements captured within each grid.

Conducting analyses with comparative indices holds significance for the practical applicability of the findings. This approach aids us in gaining a more comprehensive understanding of the variations exhibited by abiotic elements across the territory. Furthermore, it enables the interpretation of general trends and tendencies as the grid size expands. Ultimately, these insights serve to inform the potential applications of the index in the realms of territorial planning, conservation efforts, and even geotourism initiatives.

5.2. Geodiversity Patterns and Relationships between Geodiversity Classes of the Chinchiná River Basin

The analyzed geodiversity for the CRB exposed a total of 105 abiotic elements constituting 10 rock types, 7 slope ranges, 13 landforms, 5 drainage density characteristics, 9 fault kinematics, 5 soil orders, several places with an absence of soil formation processes and with anthropic soils, 11 sub-climates, 7 drainage orders, 1 underground aquifer, 4 areas with lakes, 2 glaciers, 5 polygenetic volcanoes, 22 monogenetic volcanoes, and 3 temperature ranges in hot springs. Below, an in-depth reflection is made regarding the geodiversity patterns and relationships between the elements composing the geodiversity of the CRB.

5.2.1. Lithological Sub-Index Patterns

The convergence of various types of rocks determines high lithological diversity at places in the CRB (Figure 5). In the eastern region of the basin, the highest sub-indices are primarily influenced by the confluence of Permian migmatites, the Triassic low-to-medium degree of metamorphism rocks (i.e., greenschist to amphibolite facies), Paleocene tonalites and granodiorites, Cenozoic andesites and volcanosedimentary deposits such as pyroclastic density currents, lahars, and pyroclastic falls (Figure 5). In the western region, places with high lithological diversity combine Permian migmatites with Cretaceous garnet-bearing amphibolites and lawsonite-glaucophane-actinolite schist, Mesozoic basalts, diabases, Cenozoic andesites and Mesozoic cherts, sandstones, and conglomerates (Figure 5).

In the context of the CRB, it can be argued that the distribution patterns of rocks are primarily influenced by two major geological processes that occurred in the last 250 million years: the successive adherence of terrain to the margin of the continent and the continuous volcanic–magmatic activity related to subduction processes [89,90]. The superficial sedimentary processes play minor roles, although erosion processes are favored by the steepness of the basin and the generally wet climate. The areas of high geodiversity, characterized by many lithological contacts, consist of both ancient allochthonous rocks (originating from outside the current geographic location) and recent autochthonous rocks (formed in situ within the basin). Conversely, areas with the lowest geodiversity sub-indices tend to occur within the limits of allochthonous lithological sub-classes. High lithological sub-indices are closely related to the fault tendencies identified in the basin (i.e., NE-SW, NS-NNE, NW-SE). This suggests the significant structural control of the lithological diversity distribution within the basin, although topography is also a determinant factor for the location and distribution of volcanoclastic deposits.

Overall, the high lithological diversity in the CRB (i.e., 10 abiotic elements) exposed the complexity of the tectonic evolution of the territory. The Central Cordillera in Colombia has been created over millions of years through the collision of tectonic plates, which brought together rocks of different types and formation histories in different sectors of the CRB. These processes demonstrate the dynamics of the rock cycle, which undergoes the continuous, repeated process of formation, destruction, transformation, and relocation. All these processes influence the terrestrial regulation of the basin.

5.2.2. Geomorphological Sub-Index Patterns

In the CRB, geomorphological elements are mostly concentrated along its main rivers, influenced by factors such as altitudinal gradients, abundant water, rock composition, and tectonic activity (Figure 6). Streams within the CRB act as potent agents of weathering and erosion, significantly contributing to the formation of slopes and various landforms. As water flows from higher to lower elevations, it accumulates potential energy, thus augmenting its erosive capacity and forming the pronounced valleys downstream in the basin. Various rock types interact differently with relief formation processes. For instance, in the southern region of the basin, characterized by significant geomorphological diversity, there are basement rocks and extensive volcanoclastic deposits (Figures 5 and 6). Some of these deposits are the result of ancient explosive eruptions that filled valleys and formed ignimbrites, which are prominent features in the current landscape, as they form extensive

plains and prominent scarps. Differential uplift and subsidence, resulting from faults and tectonics, introduce variations into the landscape, giving rise to a diverse range of topographic features [54]. All the geomorphological processes are also involved in the regulation geosystem services of the basin.

5.2.3. Pedological Sub-Index Patterns

The distribution patterns of soil diversity in the CRB reveal notable differences between the eastern and western regions (Figure 8). Generally, the eastern region of the basin exhibits lower soil diversity compared to the western region (Figure 8). In the eastern region, through the upper mountain, where volcanic influence is more abundant, Andisols emerge as the dominant soil type (Figure 8). However, certain areas within the basin lack significant soil development, either due to the harsh environmental conditions present at higher elevations or the presence of extensive escarpments. Additionally, Histosols, characterized by very high organic matter content, occur in wetlands and moorland systems formed along the mountainous regions. Entisols are also present, featuring an absence of well-defined pedogenic horizons, primarily due to the constant erosional dynamics observed in the channels of some intermediate-order rivers.

The areas with the highest pedological sub-indices are observed in the central and south-western regions of the basin (Figure 8). Throughout this area, besides Andisols and Entisols, Inceptisols, Mollisols, and urban soils have more constant appearances. The urban soils correspond to the places where the anthropogenic dynamics take place. This means artificial and impermeabilized soils mostly covered by concrete and other materials. The Molisols, which are very dark-colored, base-rich mineral soils, have, as parental materials, the Permian and Cretaceous metamorphic and sedimentary rocks, as well as Cenozoic alluvial materials. Inceptisols, which are usually present in active mountain landscapes, are the other abiotic pedological factor increasing the sub-index value through the CRB.

The distribution patterns of the pedological diversity sub-index reveal the interconnection between several geodiversity aspects. The incidence of parental materials, for both ancient rocks and recent volcanic activity, significantly influences soils' compositions and properties. The presence of different parent materials gives rise to a wide range of soil types. Geomorphological processes, including erosion, weathering, and sedimentation, as well as climatic conditions (i.e., temperature and precipitation), play key roles in the formation and evolution of the soils in the basin [67]. All these processes provide both regulating and supporting geosystem services in the basin.

5.2.4. Climatological Sub-Index Patterns

The distribution patterns of climatic diversity in the CRB highlight distinct variations between the eastern and western regions of the basin (Figure 9). In the eastern region, the climatic distribution exhibits two lower climatic sub-index clusters, predominantly located within the middle–high mountain areas of the Chinchiná and Guacaica sub-basins (Figure 9). On the other hand, the western region is characterized by a large and more homogeneous climatic area, primarily concentrated in the southwestern region of the basin (Figure 9). Regions characterized by climatic diversity are primarily located in the medium and high mountain areas in the eastern region, particularly centered around urban areas like Manizales and Villamaría. Additionally, climatic diversity is observed at the confluence of the Chinchiná and Guacaica rivers in the western region of the basin.

The climatic distribution pattern of the CRB exposed some relationships between the geodiversity elements shaping the local climatic conditions. Factors such as altitude, topography, faults and drainage, and rocks and soils [59,60], combined with larger-scale regional controls on the local climate [91–93], contribute to the microclimates and weather conditions observed across the basin. As elevation changes, temperature variations occur in direct proportion, as do the precipitation parameters [60]. Higher altitudes are associated with cooler temperatures, while lower elevations tend to have warmer conditions [61]. Valleys and peaks within the basin play critical roles in containing and directing humidity.

Valleys can also act as natural corridors for air masses and moisture. Processes related to climate determine the atmospheric regulating processes of the CRB.

It is crucial to recognize that there are differing opinions on whether climate should be considered a part of geodiversity. In the tropical Andean region considered in this study, climate plays a significant role in geodiversity analysis due to its frequent changes. Climate has a direct and indirect influence on various aspects of geodiversity. On one hand, long-term geological processes, like the uplifting of mountain ranges, have created the altitudinal gradient that affects climate. The combination of tectonics, rock types, and climate has also shaped the landscape. Furthermore, climate affects soil formation and is a vital component of the hydrological system. Considering climate to be a form of geodiversity helps us to understand the existing climatic conditions, which, in turn, influence the regulation and support processes in the ecosystem. The various life zones identified within the basin, characterized by their plant and animal populations, depend on the changing climatic conditions at different altitudes [61]. Moreover, understanding how global climate change impacts the region necessitates including climate as a variable in a holistic study of geodiversity. In particular, if geodiversity is fundamental for sustaining biodiversity, climate must be considered when analyzing the territory.

5.2.5. Hydrological Sub-Index Patterns

The hydrological sub-index diversity in the CRB shows a clear increasing trend along the main river channels, aligning with Strahler's drainage order method, which assigns higher values to river segments with more tributaries (Figure 10). As rivers merge and gain more tributaries, their drainage order increases, resulting in higher geodiversity values being identified in these areas. Additionally, the presence of underground aquifers in the lower basin contributes to higher sub-index values (Figure 10). In areas of high elevation, a slight increase in hydrological diversity occurs when surface lakes, such as those formed in wetlands and peat bogs and due to glacier retreat processes, are considered (Figure 10). The hydrological features of the CRB exert primarily control over the hydrological cycle, which, in turn, are related to the regulating processes of the basin.

5.2.6. Volcanological Sub-Index Patterns

The CRB exhibits a rich volcanological diversity, characterized by both polygenetic and monogenetic volcanoes (Figure 11). The distribution patterns of the volcanological diversity sub-index unveil a clear spatial tendency, with most volcanoes being clustered in the eastern region of the basin or positioned toward its central regions (Figure 11). A comparison between the eastern and western regions reveals a discernible contrast, with the highest levels of heterogeneity concentrated toward the center of the Cordillera, corresponding to the elevated regions within the basin (Figure 11). In contrast, the western region of the basin demonstrates a comparatively lower diversity of volcanoes, resulting in a more homogeneous volcanic diversity sub-index (Figure 11).

However, it is important to note that within this class, the highest sub-indexes demonstrate the concentration of volcanoes per unit area, irrespective of their type. The distribution patterns reveal that the most significant values are observed in the Chinchiná River Sub-Basin. Nevertheless, with respect to the statistical weighted procedure, the two subclasses (i.e., polygenetic and monogenetic) were used to quantify the equivalent sub-index (Table 2). All the volcanological processes expose the regulating geosystem services, and their products influence the supporting processes through the soil's formation processes, with Andisols being dominant throughout the basin.

5.2.7. Geothermal Sub-Index Patterns

The highest geothermal diversity is concentrated in the southeastern region of the basin (Figure 12). In particular, the Claro River Sub-Basin exhibits a prominent expression of geothermal diversity, characterized by a high frequency of occurrences and a wide range of temperature values. The distribution of the geothermal sub-index can be attributed to

several factors, including the proximity to polygenetic volcanoes in the southeastern region, which provide a heat source due to the presence of magmatic chambers. Additionally, structural, hydrological, and geological systems allow the surface water to infiltrate rocks, enriching it with hydrothermal fluids. In this context, a clear correlation emerges between areas characterized by high geothermal diversity and those exhibiting significant structural diversity (Figures 7 and 12).

5.2.8. Structural Geology Sub-Index Patterns

The structural diversity sub-index distribution patterns underscore the prevalence of faults, highlighting the complex tectono-structural nature of the area (Figure 7). With over half of the basin affected by faults (i.e., 610 km), it is clear that tectonic processes have significantly shaped the region. In fact, it is understandable why 87% of the basin's territory is characterized by escarpments, steep slopes, and strongly inclined terrain, as it is a byproduct of tectono-orogenesis processes of the northern Andes (Figure 7).

It is greatly important to emphasize the relationships previously identified by other authors regarding the interplay between geological structures and volcanoes [55]. This is particularly relevant as certain locations within both geodiversity classes align with areas exhibiting high geodiversity values (Figures 7 and 11). Furthermore, it is essential to emphasize the numerous faults in the region that facilitate the convergence of rocks with distinct ages, formation histories, and compositions. Additionally, it is worth underscoring the seismic risk connected to a geologically faulted territory, particularly in areas where urban development is situated above regions with significant structural diversity (Figure 7).

5.3. Final Remarks

This study identified a region with diverse and variable non-living elements. The geodiversity index highlights a basin with high geodiversity, as it contains a total of 105 different abiotic elements, converging within an area of 1051 km². Within the geographical analysis units, the highest geodiversity was observed in 1 km × 1 km areas with 27 different elements (32.5%) and in 2 km × 2 km areas with 30 elements (34.5%). It is important to note that the perception of high or low geodiversity may vary depending on the reference point, and this perception should be approached with caution when comparing indices from different studies due to methodological and contextual differences in the territories.

The geodiversity results are determined based on the quality of the mapped input data. It is noteworthy that the true geodiversity of a region always surpasses that represented in existing maps. The geodiversity index, however, offers a comprehensive analysis of the CRB's abiotic nature. The multitude of identified abiotic elements highlights a region rich in geodiverse components that collectively regulate and support a geosystem teeming with natural resources. Notably, the observed limitations related to varying scales of base cartographic information were more pronounced in the context of the geomorphological class than in regard to pedological class. This suggests that while scale is a significant factor in geodiversity indices, the inherent structure and fundamental aspects of the natural environment being assessed also play pivotal roles in determining the quantities and distributions of abiotic elements across the territory. Primarily, it becomes crucial to establish a well-defined methodological framework that contextualizes the development of the index. The subsequent statistical processing is crucial for weighing the differential impacts of classes based on their abiotic element quantities. It also allows us to determine the percentage of geodiversity present within each geographical unit of analysis. The combined application of both methods enhances the practical utility of the index.

The index uncovers valuable relationships between geodiversity elements within the CRB, illustrating intricate interconnections and interdependencies between abiotic components of nature. However, it is important to acknowledge that geodiversity is dynamic and will continually evolve as our understanding of the Earth's surface deepens. With the ongoing advancements in Earth sciences, we can identify, categorize, and incorporate new abiotic elements into the geodiversity calculation. For the CRB, future studies have the

potential to enrich the index by introducing paleontological and mineralogical data while refining the criteria used within the studied geodiversity classes.

5.4. Geodiversity as a Foundation for Sustainability

The elements of geodiversity, along with their direct and indirect interconnections, create a complex web of relationships that drive the emergence of geosystem services, which play vital roles in performing essential physical and chemical functions within the CRB. This network of relationships forms the foundation of the basin's natural system, defining the geosystem services that, in turn, regulate, support, and provide life-sustaining resources within its territory [94].

Considering the relationships and distribution patterns detailed above, the following subsection is a contribution for a region that urgently needs to include sustainability practices in the management of its territory, mainly because it is experiencing challenging geosystemic alterations in structure and functionality of its environment. This is especially concerning in the southeastern region of the basin, where medium-to-high levels of geodiversity have been identified (Figure 13). In this area, the natural processes related to water and climate in the high-altitude mountains are critical for supporting life in the basin [95]. Unfortunately, these processes are under threat due to climate change and the loss of important geological features like equatorial glaciers (Figure 14). Poor land management practices at the local level are worsening this situation (Figure 14).

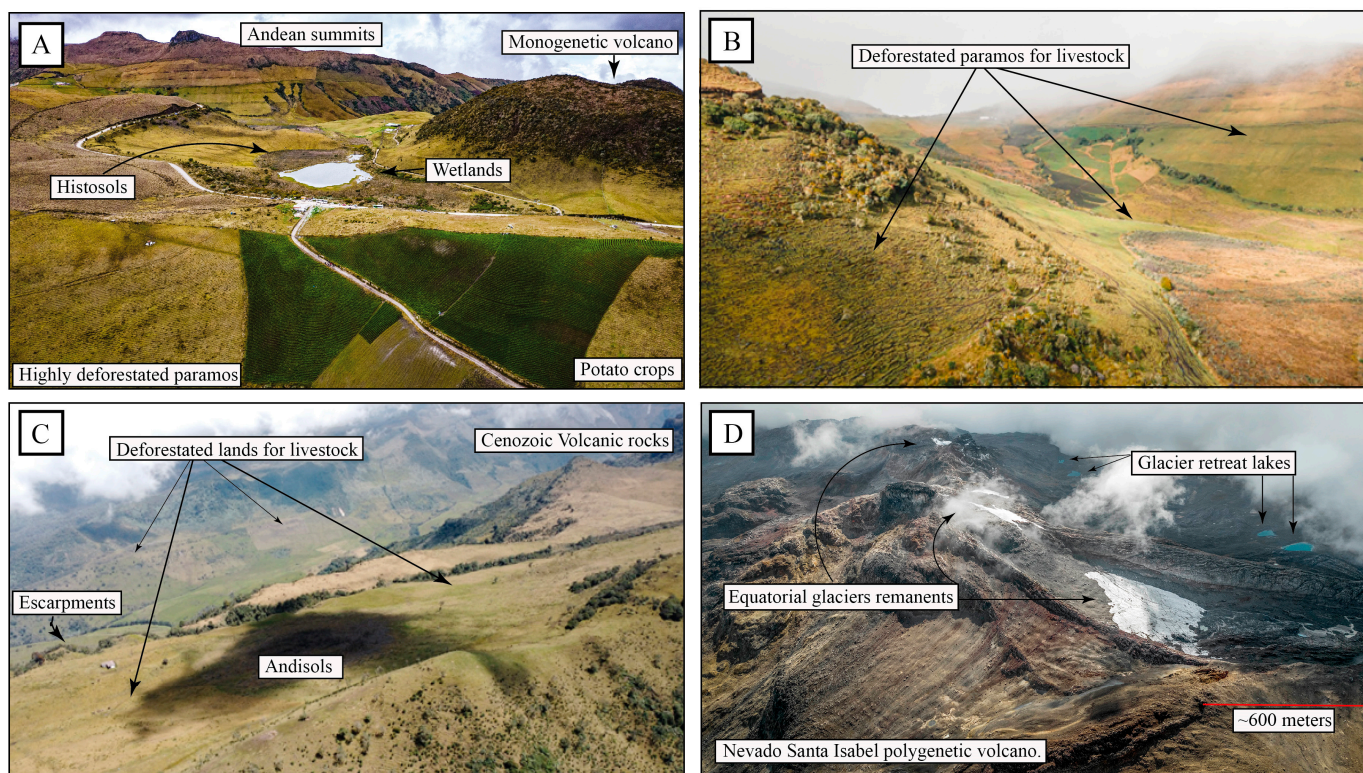


Figure 14. Aerial photographs of the high mountain landscapes and climate change scenarios. (A–C) Extensive deforested paramo lands. (D) Glacier retreat process of the Nevado Santa Isabel Volcano. Photo credits: (14A,B: AURORA, Sciences Communications; C: Miguel Uribe; D: Gustavo Acosta).

In this area, there are intricate relationships between various natural elements, such as rocks, soil, landforms, water, climate, faults, and volcanoes (Figure 14). These interactions have given rise to unique ecosystems called “paramos”, which are of utmost importance, since they play vital roles in storing water and supporting distinctive plant life [96]. Within these high-altitude regions, characterized by medium-to-high geodiversity values, several abiotic elements are at risk, with some even facing the threat of extinction, like the high

mountain glaciers (Figure 14D). Furthermore, human activities, such as deforestation, are rapidly reducing forest cover in the watershed (Figure 14A–C). These activities have a profound impact on critical ecological functions, such as water storage, the accumulation of organic matter, and the regulation of water through processes like evaporation and evapotranspiration. These changes not only disrupt local climate regulation but also have far-reaching effects on the broader ecosystem. Reduced humidity, rising temperatures, and increased soil erosion and degradation are some of the consequences, all of them abiotic elements or factors influencing geodiversity. At stake here is the potential loss of essential natural components crucial for maintaining the region's biodiversity and, consequently, the proper functioning of its ecosystems, culture, and basic necessities, particularly in the high-altitude mountain areas.

In this context, our research delivers a compelling call to action, urging the region to address both global and local climatic changes that pose threats to the well-being of the basin's geosystemic processes. Drawing on the geodiversity meticulously described and quantified in this study serves as a foundational pillar for the development of the sustainable territorial strategy currently underway: the UNESCO World Geopark project known as "Volcán del Ruiz" (<https://geoparquevolcandelruiz.com/>) (accessed on 9 September 2023). This project hinges on the universal principles that underpin strategies encompassing geoconservation, geotourism, and geoeducation. Its aim is to bring the richness of geodiversity closer to the local community, preserving its invaluable natural geological heritage while elevating the cultural values that are integral to a region deeply reliant on the geosystem's health for its continued livability.

6. Conclusions

The quantitative analysis of the CRB reveals 8 geodiversity classes, 28 geodiversity subclasses, and 105 abiotic elements composed of 10 rock types, 7 slope ranges, 13 landforms, 5 drainage density features, 9 fault kinematics, 5 soil orders, several places with an absence of soil formation processes and places with anthropic soils, 11 sub-climates, 7 drainage orders, 1 underground aquifer, 4 areas with lakes, 2 glaciers, 5 polygenetic volcanoes, 22 monogenetic volcanoes, and 3 temperature ranges in hot springs. All of them converge along 1051 km² thanks to multiple interconnected geosystemic processes that regulate, support, and carry out the development of life within the CRB.

The calculated geodiversity index is significantly influenced by geomorphology, primarily due to methodological constraints related to scale and the inherent natural variations in the mountainous environment of the CRB. It is essential to note that this index identifies areas with the greatest abiotic diversity along the Chinchiná and Claro rivers, situated in both the central and southern regions of the basin. These high-geodiversity regions contain a variety of features, including volcanoes, hot springs, glaciers, lakes, and aquifers. Moreover, other classes contribute by distributing abiotic elements throughout the entire basin, such as lithologies, soils, and climate.

The statistical processing proposed for determining the equivalent weights of geodiversity classes in relation to the total geodiversity within a territory enhances our ability to interpret geodiversity. In the context of the CRB, it revealed that areas with the highest geodiversity, as defined by units of analysis at 1 km × 1 km and 2 km × 2 km, account for over 30% of the basin's abiotic elements. Conversely, regions with lower geodiversity represent approximately 10% of the basin's abiotic elements. Combining statistical processing with the integration of indices provides a versatile tool for various applications related to territorial use, such as geoconservation, territorial planning, or geotourism. This integration enhances the index's practicality and relevance, since it demonstrates the variability in geodiversity across the territory.

The computed geodiversity sub-indices revealed interesting correlations between the abiotic elements within the CRB geodiversity. Analyzing these interconnections is imperative for understanding the regulation and support processes that facilitate the provision of culture and knowledge among the basin's inhabitants. Furthermore, comparing the index-

based information with the observed natural world is of great significance, as it assists in unraveling the structure and functioning of the geosystems. Notably, within the CRB, a high mountain area has been identified, characterized by remarkable geological diversity. This region plays a crucial role in hosting hydroclimatic and terrestrial regulatory processes vital for sustaining life within the basin, processes that are currently facing disruptions due to both global climate change and land use practices in the high mountain region, which are primarily dedicated to livestock and agriculture.

Basing territorial sustainability strategies on the comprehensive insights derived from geodiversity studies is indispensable for fostering an integrated understanding of geosystems. Specifically, projects similar to the UNESCO World Geoparks, such as the “Volcán del Ruiz” project taking place in our region, offer a valuable chance to connect the knowledge that we have gained through the study of geodiversity. These projects focus on preserving our natural resources through geoconservation, teaching about how everything is interconnected via geoeeducation, and making the most of our cultural values for people to enjoy and appreciate through geotourism. This, indeed, puts the primary advantages of geosystem services in perspective, particularly in the realm of cultural and knowledge services.

Author Contributions: Conceptualization, A.A.-D., H.M. and F.V.-H.; methodology, A.A.-D.; software, A.A.-D.; validation, A.A.-D.; formal analysis, A.A.-D.; investigation, A.A.-D.; resources, A.A.-D., H.M. and K.N.; data curation, A.A.-D. and H.M.; writing—original draft preparation, A.A.-D., H.M. and F.V.-H.; writing—review and editing, A.A.-D., H.M., F.V.-H. and K.N.; visualization, A.A.-D.; supervision, H.M., F.V.-H. and K.N.; project administration, A.A.-D. and H.M. All authors have read and agreed to the published version of the manuscript.

Funding: This study is part of the project: MINCIENCIAS (call 890, 2020), Colombia: “Vulcanismo en el centro y suroccidente del país: Implicaciones de origen, evolución, amenaza, relación con el desarrollo de suelos volcánicos y potencial geoturístico. Alejandro Arias has been partially financed by Alcaldía de Manizales, Caldas, Colombia: (call “Manizales + innovadora” cohorte II).

Data Availability Statement: All data are included in the main text.

Acknowledgments: We offer special thanks to the researchers, technicians, and administrative staff of the Instituto de Investigaciones en Estratigrafía (IIES) for their support. We also offer thanks to Sergio Gómez (FollowVideos), Gustavo Acosta, and Miguel Uribe for providing pictures, and Geoffrey Lerner for helping us with a review of the English language used. Finally, we are grateful to the reviewers because their valuable suggestions helped to improve the manuscript.

Conflicts of Interest: The authors declare no conflict of interest.

References

1. Kozłowski, S. Geodiversity. The concept and scope of geodiversity. *Przegląd Geol.* **2004**, *52*, 833–837.
2. Carcavilla Urquí, L.; Lopez-Martínez, J.; Durán-Valsero, J.J. *Patrimonio Geológico y Geodiversidad: Investigación, Conservación, Gestión y Relación con los Espacios Naturales Protegidos (No. 7)*; IgmE: Madrid, Spain, 2007.
3. Serrano, E.; Ruiz-Flaño, P. Geodiversity: A theoretical and applied concept. *Geogr. Helv.* **2007**, *62*, 140–147. [[CrossRef](#)]
4. Gray, M. The confused position of the geosciences within the “natural capital” and “ecosystem services” approaches. *Ecosyst. Serv.* **2018**, *34*, 106–112. [[CrossRef](#)]
5. Brilha, J.; Gray, M.; Pereira, D.; Pereira, P. Geodiversity: An integrative review as a contribution to the sustainable management of the whole of nature. *Environ. Sci. Policy* **2018**, *86*, 19–28. [[CrossRef](#)]
6. Hjort, J.; Gordon, J.E.; Gray, M.; Hunter, M.L., Jr. Why geodiversity matters in valuing nature’s stage. *Conserv. Biol.* **2015**, *29*, 630–639. [[CrossRef](#)] [[PubMed](#)]
7. Van Ree, C.C.; van Beukering, P.J. Geosystem services: A concept in support of sustainable development of the subsurface. *Ecosyst. Serv.* **2016**, *20*, 30–36. [[CrossRef](#)]
8. Gray, M. *Geodiversity: Valuing and Conserving Abiotic Nature*; John Wiley & Sons: Hoboken, NJ, USA, 2004.
9. Gray, M. Geodiversity: Developing the paradigm. *Proc. Geol. Assoc.* **2008**, *119*, 287–298. [[CrossRef](#)]
10. Gordon, J.E.; Barron, H.F. The role of geodiversity in delivering ecosystem services and benefits in Scotland. *Scott. J. Geol.* **2013**, *49*, 41–58. [[CrossRef](#)]
11. Gordon, J.E.; Barron, H.F.; Hanson, J.D.; Thomas, M.F. Engaging with geodiversity—Why it matters. *Proc. Geol. Assoc.* **2012**, *123*, 1–6. [[CrossRef](#)]

12. Yu, Y.; Yang, J. The Role and Practice of Geodiversity in Serving Ecosystems in China. *Sustainability* **2022**, *14*, 4547. [[CrossRef](#)]
13. Van Ree, C.C.D.F.; Van Beukering, P.J.H.; Boekstijn, J. Geosystem services: A hidden link in ecosystem management. *Ecosyst. Serv.* **2017**, *26*, 58–69. [[CrossRef](#)]
14. Zwoliński, Z.; Najwer, A.; Giardino, M. Methods for assessing geodiversity. In *Geoheritage*; Elsevier: Amsterdam, The Netherlands, 2018; pp. 27–52.
15. Benito-Calvo, A.; Pérez-González, A.; Magri, O.; Meza, P. Assessing regional geodiversity: The Iberian Peninsula. *Earth Surf. Process. Landf.* **2009**, *34*, 1433–1445. [[CrossRef](#)]
16. Zwoliński, Z. The routine of landform geodiversity map design for the Polish Carpathian Mts. *Landf. Anal.* **2009**, *11*, 77–85.
17. Hjort, J.; Luoto, M. Geodiversity of high-latitude landscapes in northern Finland. *Geomorphology* **2010**, *115*, 109–116. [[CrossRef](#)]
18. Ruban, D.A. Quantification of geodiversity and its loss. *Proc. Geol. Assoc.* **2010**, *121*, 326–333. [[CrossRef](#)]
19. Pellitero, R.; González-Amuchastegui, M.J.; Ruiz-Flaño, P.; Serrano, E. Geodiversity and geomorphosite assessment applied to a natural protected area: The Ebro and Rudron Gorges Natural Park (Spain). *Geoheritage* **2011**, *3*, 163–174. [[CrossRef](#)]
20. Silva, J.P.; Pereira, D.I.; Aguiar, A.M.; Rodrigues, C. Geodiversity assessment of the Xingu drainage basin. *J. Maps* **2013**, *9*, 254–262. [[CrossRef](#)]
21. Pereira, D.I.; Pereira, P.; Brilha, J.; Santos, L. Geodiversity assessment of Paraná State (Brazil): An innovative approach. *Environ. Manag.* **2013**, *52*, 541–552. [[CrossRef](#)]
22. Argyriou, A.V.; Sarris, A.; Teeuw, R.M. Using geoinformatics and geomorphometrics to quantify the geodiversity of Crete, Greece. *Int. J. Appl. Earth Obs. Geoinf.* **2016**, *51*, 47–59. [[CrossRef](#)]
23. Forte, J.P.; Brilha, J.; Pereira, D.I.; Nolasco, M. Kernel density applied to the quantitative assessment of geodiversity. *Geoheritage* **2018**, *10*, 205–217. [[CrossRef](#)]
24. Vörös, F.; Pál, M.; van Wyk de Vries, B.; Székely, B. Development of a New Type of Geodiversity System for the Scoria Cones of the Chaîne des Puys Based on Geomorphometric Studies. *Geosciences* **2021**, *11*, 58. [[CrossRef](#)]
25. Zakharovskiy, V.; Németh, K. Scale influence on qualitative–quantitative geodiversity assessments for the geosite recognition of Western Samoa. *Geographies* **2022**, *2*, 476–490. [[CrossRef](#)]
26. Scammacca, O.; Bétard, F.; Aertgeerts, G.; Heuret, A.; Fermet-Quinet, N.; Montagne, D. Geodiversity assessment of French Guiana: Challenges and implications for sustainable land planning. *Geoheritage* **2022**, *14*, 83. [[CrossRef](#)]
27. Pérez-Escobar, O.A.; Zizka, A.; Bermúdez, M.A.; Meseguer, A.S.; Condamine, F.L.; Hoorn, C.; Hooghiemstra, H.; Pu, Y.; Bogarín, D.; Boschman, L.M.; et al. The Andes through time: Evolution and distribution of Andean floras. *Trends Plant Sci.* **2022**, *27*, 364–378. [[CrossRef](#)] [[PubMed](#)]
28. Carrascal, D.R.; Maya, M.D.P.A.; Elena, M.; Lagoueyte, G.; Jaramillo, P.A.Z. Increased climatic stress on high-Andean ecosystems in the Cordillera Central of Colombia. *About SCOPE* **2011**, 182.
29. IDEAM. *Zonificación y Codificación de Unidades Hidrográficas e Hidrogeológicas de Colombia*; Publicación aprobada por el Comité de Comunicaciones y Publicaciones de IDEAM: Bogotá, Colombia, 2013.
30. Perez-Valvueda, G.J.; Arrieta-Arrieta, A.M.; Contreras-Anaya, J.G. Río Cauca: La Geografía Económica de su Área de Influencia. In *Documentos de Trabajo Sobre Economía Regional*; Banco de la Republica de Colombia, Centro de estudios regionales (CEER): Bogotá, Colombia, 2015.
31. Etayo-Serna, F.; Barrero, D.; Lozano, H.; Espinosa, A.; González, H.; Orrego, A.; Ballesteros, I.; Forero, H.; Ramírez, C.; Zambrano-Ortiz, F.; et al. *Mapa de Terrenos Geológicos de Colombia*; Publicaciones Geológicas Especiales del Ingeominas: Bogotá, Colombia, 1983; Volume 14, pp. 1–135.
32. Restrepo, J.J.; Toussaint, J.F. Terranes and continental accretion in the Colombian Andes. *Episodes* **1988**, *11*, 189–193. [[CrossRef](#)]
33. Toussaint, J.F.; Restrepo, J.J. Acreciones sucesivas en Colombia: Un nuevo modelo de evolución geológica. In *V Congreso Colombiano de Geología. Memoirs, I*; Cartec Ltd.a: Bucaramanga, Colombia, 1989; pp. 127–146.
34. Restrepo, J.J.; Toussaint, J.F. Tectonostratigraphic Terranes in Colombia: An Update First Part: Continental Terranes. In *Geology of Colombia, Volume 1. Proterozoic—Paleozoic*; Gómez, J., Mateus-Zabala, D., Eds.; Servicio Geológico Colombiano, Publicaciones Geológicas Especiales: Bogotá, Colombia, 2020.
35. Trenkamp, R.; Kellogg, J.N.; Freymueller, J.T.; Mora, H.P. Wide plate margin deformation, southern Central America and northwestern South America, CASA GPS observations. *J. South Am. Earth Sci.* **2002**, *15*, 157–171. [[CrossRef](#)]
36. Kobayashi, D.; LaFemina, P.; Geirsson, H.; Chichaco, E.; Abrego, A.A.; Mora, H.; Camacho, E. Kinematics of the western Caribbean: Collision of the Cocos Ridge and upper plate deformation. *Geochem. Geophys. Geosystems* **2014**, *15*, 1671–1683. [[CrossRef](#)]
37. Mora-Páez, H.; Kellogg, J.N.; Freymueller, J.T.; Mencin, D.; Fernandes, R.M.; Diederix, H.; LaFemina, P.; Cardona-Piedrahita, L.; Lizarazo, S.; Peláez-Gaviria, J.-R.; et al. Crustal deformation in the northern Andes—A new GPS velocity field. *J. South Am. Earth Sci.* **2019**, *89*, 76–91. [[CrossRef](#)]
38. Kellogg, J.N.; Camelio, G.B.F.; Mora-Páez, H. Cenozoic tectonic evolution of the North Andes with constraints from volcanic ages, seismic reflection, and satellite geodesy. In *Andean Tectonics*; Elsevier: Amsterdam, The Netherlands, 2019; pp. 69–102.
39. Gómez-Tapias, J.; Núñez-Tello, A.; Mateus-Zabala, D.; Alcárcel-Gutiérrez, F.A.; Lasso-Muñoz, R.M.; Marín-Rincón, E.; Marroquín-Gómez, M.P. Physiographic and geological setting of the Colombian territory. *Geol. Colomb.* **2020**, *1*, 1–6.
40. Monsalve-Bustamante, M.L.; Gómez, J.; Pinilla-Pachon, A.O. The volcanic front in Colombia: Segmentation and recent and historical activity. *Geol. Colomb.* **2020**, *4*, 97–159.

41. Gómez, J.; Montes, N.E.; Nivia, A.; Diederix, H.; Compiladores. Mapa Geológico de Colombia 2015. Escala 1:1,000,000. Servicio Geológico Colombiano, 2 hojas. Bogotá. 2015. [CrossRef]
42. Stern, C.R. Active Andean volcanism: Its geologic and tectonic setting. *Rev. Geológica Chile* **2004**, *31*, 161–206. [CrossRef]
43. Martínez, L.; Valencia, L.; Ceballos, J.; Narváez, B.; Pulgarín, B.; Correa, A.; Navarro, S.; Murcia, H.; Zuluaga, I.; Rueda, J.; et al. Geología y estratigrafía del Complejo Volcánico Nevado del Ruiz. In *Informe Final, Bogotá—Manizales—Popayán*; Servicio Geológico Colombiano: Bogotá, Colombia, 2014; 853p.
44. Murcia, H.; Borrero, C.; Németh, K. Overview and plumbing system implications of monogenetic volcanism in the northernmost Andes' volcanic province. *J. Volcanol. Geotherm. Res.* **2019**, *383*, 77–87. [CrossRef]
45. International Commission on Geoheritage of the International Union of Geological Sciences (IGC-IUGS), Designations. 2023. Available online: https://iugs-geoheritage.org/geoheritage_sites/nevado-del-ruiz-quaternaly-volcanic-complex (accessed on 7 September 2023).
46. Botero-Gómez, L.A.; Osorio, P.; Murcia, H.; Borrero, C.; Grajales, J.A. Campo Volcánico Monogenético Villamaría-Termale, Cordillera Central, Andes colombianos (Parte I): Características morfológicas y relaciones temporales. *Boletín Geol.* **2018**, *40*, 85–102. [CrossRef]
47. Osorio, P.; Botero-Gómez, L.A.; Murcia, H.; Borrero, C.; Grajales, J.A. Campo Volcánico Monogenético Villamaría-Termale, Cordillera Central, Andes colombianos (Parte II): Características composicionales. *Boletín Geol.* **2018**, *40*, 103–123. [CrossRef]
48. Marín-Cerón, M.I.; Leal-Mejía, H.; Mesa-García, J. Late Cenozoic to modern-day volcanism in the northern Andes: A geochronological, petrographical, and geochemical review. In *Geology and Tectonics of Northwestern South America: The Pacific-Caribbean-Andean Junction*; Cediél, F., Shaw, R.P., Eds.; Springer International Publishing: Berlin/Heidelberg, Germany, 2019; pp. 3–95.
49. Ceballos-Hernández, J.A.; Martínez-Tabares, L.M.; Valencia-Ramírez, L.G.; Pulgarín-Alzate, B.A.; Correa-Tamayo, A.M.; Narváez-Marulanda, B.L.; Gómez, J.; Pinilla-Pachon, A.O. Geological evolution of the Nevado del Ruiz Volcanic Complex. *Geol. Colomb.* **2020**, *4*, 267–296.
50. Salazar-Muñoz, N.; de la Ossa, C.A.R.; Murcia, H.; Schonwalder-Ángel, D.; Botero-Gómez, L.A.; Hincapié, G.; da Silva, J.C.; Sánchez-Torres, L. Andesitic (SiO₂: ~60 wt%) monogenetic volcanism in the northern Colombian Andes: Crystallisation history of three Quaternary volcanoes. *J. Volcanol. Geotherm. Res.* **2021**, *412*, 107194. [CrossRef]
51. Vargas-Arcila, L.; Murcia, H.; Osorio-Ocampo, S.; Sánchez-Torres, L.; Botero-Gómez, L.A.; Bolaños, G. Effusive and evolved monogenetic volcanoes: Two newly identified (~800 ka) cases near Manizales City, Colombia. *Bull. Volcanol.* **2023**, *85*, 42. [CrossRef]
52. Vargas-Arcila, L. Caracterización de Los Volcanes Las Margaritas 1 y 2, Campo Volcánico Monogenético Tapias-Guacaica, Colombia. Bachelor's Thesis, Universidad de Caldas, Caldas, Colombia, 2020.
53. Raigosa-Riobó, S. Aporte a Los Estudios Cartográficos, Composicionales y Geocronológicos del Campo Volcánico Monogéntico Tapias-Guacaica Municipio de Neira, Caldas, Colombia. Bachelor's Thesis, Universidad de Caldas, Caldas, Colombia, 2021.
54. Florez, A. Geomorphology of the Manizales—Chinchiná Area Cordillera Central, Colombia. Ph.D. Thesis, University of Amsterdam, Amsterdam, The Netherlands, 1986.
55. Botero-Gómez, L.A. Control Estructural y Relación Temporal de los Volcanes Pertenecientes al Campo Volcánico Monogenético Villamaría-Termale, Caldas, Colombia. Master's Thesis, Universidad de Caldas, Caldas, Colombia, 2022.
56. Ortiz, I.; Alfaro, C. *Inventario Nacional de Manantiales Termale. Fase 2011*; Informe Técnico: Bogotá, Colombia, 2011; 131p.
57. Taborda, A.; Portela, J.P.; Lopez-Sanchez, J.; Daniele, L.; Moreno, D.; Blessent, D. Temperature estimation of the Nevado del Ruiz Volcano geothermal reservoir: Insight from western hot springs hydrogeochemistry. *J. Geochem. Explor.* **2022**, *240*, 107049. [CrossRef]
58. Inguaggiato, C.; Censi, P.; Zuddas, P.; Londoño, J.; Chacón, Z.; Alzate, D.; Brusca, L.; D'alessandro, W. Geochemistry of REE, Zr and Hf in a wide range of pH and water composition: The Nevado del Ruiz volcano-hydrothermal system (Colombia). *Chem. Geol.* **2015**, *417*, 125–133. [CrossRef]
59. Jaramillo-Robledo, A. *Clima Andino y Café en Colombia*; Chinchiná: Cenicafé, Colombia, 2005; 196p.
60. Ocampo-López, O.L. Análisis de Vulnerabilidad de la Cuenca del Río Chinchiná para Condiciones Estacionarias y de Cambio Climático. Master's Thesis, Universidad Nacional de Colombia, Caldas, Colombia, 2012.
61. CORPOCALDAS; ASOCARS; Universidad Nacional de Colombia. *Plan de Ordenación y Manejo Ambiental de la Cuenca Hidrográfica del Río Chinchiná en el Departamento de Caldas—Colombia*; Colombian Government: Caldas, Colombia, 2013.
62. Ceballos, J.L. Manifestación de Cambio Climático—Los Glaciares de Colombia. *Revista La Tadeo (Cesada a Partir De 2012)*, (74). Recuperado a Partir de. 2009. Available online: <https://revistas.utadeo.edu.co/index.php/RLT/article/view/516> (accessed on 25 June 2022).
63. Valentin, C.D. Desarrollo de una Herramienta de ArcGis Para el Cálculo de la Geodiversidad en Latinoamérica, y su Análisis Estadístico y de Correlación con las Amenazas en un Caso de Estudio. Master's Thesis, Universidad Autónoma de Mexico, Mexico City, Mexico, 2021.
64. Caballero, H.; Zapata, G. *Geología y Geoquímica de la Plancha 224 Pereira*; Informe 1931; INGEOMINAS: Medellín, Colombia, 1984.
65. Gonzalez, H. *Geología de las Planchas 206 Manizales y 225 Nevado del Ruiz*; Memoria explicative; Instituto de Investigación e Información Geocientífica, Minero-Ambiental y Nuclear, INGEOMINAS: Medellín, Colombia, 2001; 89p.
66. Estrada, J.J.; Viana, R.; Gonzalez, H. *Geología de la Plancha 205 Chinchiná*; Memoria explicative; Instituto de Investigación e Información Geocientífica, Minero-Ambiental y Nuclear, INGEOMINAS: Medellín, Colombia, 2001; 93p.

67. IGAC; CORPOCALDAS. *Estudio Semidetallado de Suelos de los Municipios de Manizales, Chinchiná, Palestina, Neira y Villamaría*; Escala 1:25.000. Republica de Colombia; Colombian Government: Caldas, Colombia, 2013.
68. Aguirre-Sánchez, R.; López-Isaza, J.A. *Cartografía Geológica y Petrografía del Stock de Manizales y su Relación con sus Rocas Encajantes*. Bachelor's Thesis, Universidad de Caldas, Caldas, Colombia, 2003.
69. Montenegro-Rippe, C.A. *Caracterización Petrográfica del Stock de Manizales*. Master's Thesis, Universidad Nacional de Colombia, Bogotá, Colombia, 2017.
70. Álvarez, J.A. Geología del Complejo Ofiolítico de Pácora y secuencias relacionadas de Arco de Islas (Complejo quebrada Grande), Colombia. *Boletín Geológico* **1995**, *35*, 5–49. [[CrossRef](#)]
71. Rodríguez, G.; Arango, M.I. Reinterpretación geoquímica y radiométrica de las metabasitas del Complejo Arquía. *Boletín Geol.* **2013**, *35*, 65–81.
72. Leal-Mejía, H.; Shaw, R.P.; Melgarejo i Draper, J.C. Spatial-temporal migration of granitoid magmatism and the Phanerozoic tectono-magmatic evolution of the Colombian Andes. In *Geology and Tectonics of Northwestern South America: The Pacific-Caribbean-Andean Junction*; Springer: Berlin/Heidelberg, Germany, 2019; pp. 253–410.
73. Maya, M.; González, H. Unidades litodémicas en Cordillera Central de Colombia. *Bol. Geol. Boletín Geológico* **1995**, *35*, 44–57. [[CrossRef](#)]
74. Moreno-Sanchez, M.; Pardo-Trujillo, A. Stratigraphical and sedimentological constraints on western Colombia: Implications on the evolution of the Caribbean plate. In *The Circum-Gulf of Mexico and the Caribbean: Hydrocarbon Habitats, Basin Formation and Plate Tectonics*; American Association of Petroleum Geologists: Tulsa, OK, USA, 2003.
75. Villagómez, D.; Spikings, R. Thermochronology and tectonics of the Central and Western Cordilleras of Colombia: Early Cretaceous–Tertiary evolution of the northern Andes. *Lithos* **2013**, *160*, 228–249. [[CrossRef](#)]
76. Moreno Sánchez, M.; Gómez Cruz, A.D.J.; Castillo González, H. Ocurrencias de fosiles Paleozoicos al este de la parte norte de la Cordillera Central y discusion sobre su significado geologico. *Boletín Cienc. Tierra* **2008**, *22*, 39–47.
77. Pardo-Trujillo, A.; Moreno, M.; Gómez, A.D.J. The Nogales Formation in the edge of the central mountain chain (cauca valley departament): A key piece to understand the Cretaceous evolution of west colombian. *Boletín Cienc. Tierra* **2008**, *22*, 133.
78. Ossa, J.A. *Cartografía Detallada de un Área del Proyecto Geotérmico*. Bachelor's Thesis, Facultad de Ciencias Exactas y Naturales, Programa de Geología, Universidad de Caldas, Manizales, Colombia, 2018; 91p.
79. Acuña, B.; Guerrero, C. *Cartografía y Análisis Cinemático de la Falla Cauca—Almaguer al Occidente de la Ciudad de Manizales*. Bachelor's Thesis, Facultad de Ciencias Exactas y Naturales, Programa de Geología, Universidad de Caldas, Manizales, Colombia, 2017; 76p.
80. Mejía Toro, E.L. *Características Cinemáticas y Condiciones de Deformación de un Segmento de la Falla Palestina al NE del Volcán Nevado del Ruiz*. Master's Thesis, Universidad Nacional de Colombia, Departamento de Geociencias, Medellín, Colombia, 2012.
81. Arango, M. *Análisis Deformativo y Cinemático de la Falla Santa Rosa. Sector Cerro Gualí—Mariquita*. Bachelor's Thesis, Facultad de Ciencias Exactas y Naturales, Programa de Geología, Universidad de Caldas, Manizales, Colombia, 2016; 64p.
82. Pareja, E.; García, R. *Análisis Estructural de la Falla NEREIDAS, en el sector de Nereidas, Villamaría—Caldas*. Bachelor's Thesis, Facultad de Ciencias Exactas y Naturales, Programa de Geología, Universidad de Caldas, Manizales, Colombia, 2013.
83. Gómez, E.; Marín, J.S. *Análisis de Paleofuerzos Mediante Datos de Fallas Estriadas en el “Stock” Chinchiná—Santa Rosa, Alrededores de Manizales*. Bachelor's Thesis, Facultad de Ciencias Exactas y Naturales, Programa de Geología, Universidad de Caldas, Manizales, Colombia, 2014; 62p.
84. Vega, E.J. *Aporte al Modelo Geológico del Valle de las Nereidas, Villamaría*. Bachelor's Thesis, Universidad de Caldas, Facultad de Ciencias Exactas y Naturales, Programa de geología, Manizales, Colombia, 2014.
85. USDA Taxonomy. *A Basic System of Soil Classification for Making and Interpreting Soil Surveys*. In *Handbook No. 436*; US Department of Agriculture: Washington, WA, USA, 1999.
86. Zapata, O.E.C.; Serna, R.J. *Contribución al Modelo Hidrogeológico del Sistema Acuífero de Santágueda, Departamento de Caldas*. Bachelor's Thesis, Facultad de Ciencias Exactas y Naturales, Programa de Geología, Universidad de Caldas, Manizales, Colombia, 2012.
87. Bartuś, T. Basic unit size in the analysis of the distribution of spatial landscape elements on the basis of the lithostratigraphic geodiversity of the Ojców National Park (Poland). *Geol. Geophys. Environ.* **2017**, *43*, 95. [[CrossRef](#)]
88. Lopes, C.; Teixeira, Z.; Pereira, D.I.; Pereira, P. Identifying Optimal Cell Size for Geodiversity Quantitative Assessment with Richness, Diversity and Evenness Indices. *Resources* **2023**, *12*, 65. [[CrossRef](#)]
89. Blanco-Quintero, I.F.; García-Casco, A.; Toro, L.M.; Moreno, M.; Ruiz, E.C.; Vinasco, C.J.; Morata, D. Late Jurassic terrane collision in the northwestern margin of Gondwana (Cajamarca Complex, eastern flank of the Central Cordillera, Colombia). *Int. Geol. Rev.* **2014**, *56*, 1852–1872. [[CrossRef](#)]
90. Villagómez, D.; Spikings, R.; Magna, T.; Kammer, A.; Winkler, W.; Beltrán, A. Geochronology, geochemistry and tectonic evolution of the Western and Central cordilleras of Colombia. *Lithos* **2011**, *125*, 875–896. [[CrossRef](#)]
91. Hoyos, I.; Dominguez, F.; Cañón-Barriga, J.; Martínez, J.A.; Nieto, R.; Gimeno, L.; Dirmeyer, P.A. Moisture origin and transport processes in Colombia, northern South America. *Clim. Dyn.* **2018**, *50*, 971–990. [[CrossRef](#)]
92. Poveda, G.; Mesa, O.J. On the existence of Lloró (the rainiest locality on Earth): Enhanced ocean-land-atmosphere interaction by a low-level jet. *Geophys. Res. Lett.* **2000**, *27*, 1675–1678. [[CrossRef](#)]
93. Urrea, V.; Ochoa, A.; Mesa, O. Seasonality of rainfall in Colombia. *Water Resour. Res.* **2019**, *55*, 4149–4162. [[CrossRef](#)]

94. Fox, N.; Graham, L.J.; Eigenbrod, F.; Bullock, J.M.; Parks, K.E. Incorporating geodiversity in ecosystem service decisions. *Ecosyst. People* **2020**, *16*, 151–159. [[CrossRef](#)]
95. Buytaert, W.; Vuille, M.; Dewulf, A.; Urrutia, R.; Karmalkar, A.; Céleri, R. Uncertainties in climate change projections and regional downscaling in the tropical Andes: Implications for water resources management. *Hydrol. Earth Syst. Sci.* **2010**, *14*, 1247–1258. [[CrossRef](#)]
96. Sevink, J.; Hofstede, R. Los árboles como elemento importante del páramo. In *Avances en Investigación para la Conservación de los Páramos Andinos*; CONDESAN: Lima, Perú, 2014.

Disclaimer/Publisher’s Note: The statements, opinions and data contained in all publications are solely those of the individual author(s) and contributor(s) and not of MDPI and/or the editor(s). MDPI and/or the editor(s) disclaim responsibility for any injury to people or property resulting from any ideas, methods, instructions or products referred to in the content.